https://doi.org/10.5194/egusphere-2026-551
Preprint. Discussion started: 20 March 2026

Benchmarking a new urban scheme in the ORCHIDEE v2.2 land surface model

Morgane Lalonde[1, 2, 3], Sophie Bastin[1], Ludovic Oudin[2], Pedro Felipe Arboleda-Obando[2], Agnès Ducharne[2]

[1]LATMOS/IPSL, UVSQ Université Paris-Saclay, Sorbonne Université, CNRS, Guyancourt, France
[2]Sorbonne Université, CNRS, EPHE, UMR METIS, Paris, France
[3]Institute for Atmospheric and Climate Science, ETH Zürich, Zurich, Switzerland

Correspondence to: Morgane Lalonde (morgane.lalonde@env.ethz.ch)

Abstract. Urban areas change natural surface energy and water balances, yet some land surface models still represent cities as natural surfaces. In this study, we present the development of a one-tile urban scheme for the ORCHIDEE land surface model, designed to improve the representation of urban processes, particularly for high-resolution applications. The scheme incorporates key urban parameters such as albedo, building height, thermal properties, and imperviousness. We propose a novel physically-based approach for representing imperviousness, by modifying saturated hydraulic conductivity to account for both surface and subsurface impacts. Off-line simulations across 20 urban flux tower sites show improved performance in sensible and latent heat fluxes with the new urban scheme, compared to the original baresoil representation. Mean absolute error (MAE) evaluation confirms improved model skill, aligning with benchmark results from the Urban-PLUMBER intercomparison. The scheme also captures expected urban hydrological signatures, such as increased runoff, though some reductions in drainage may be less consistent with observed urban recharge patterns. This work lays the foundation for applying ORCHIDEE at the basin scale and in high-resolution convection-permitting for urban hydroclimate studies. Perspectives include refining thermal parameter choices, integrating anthropogenic heat fluxes, and conducting high-resolution simulations to assess hydrological performances using observed streamflow data.

1 Introduction

Land Surface Models (LSMs) simulate surface processes such as the surface energy and water budgets and are designed to be coupled to atmospheric models, with an emphasis on robust land–atmosphere exchanges across diverse environments (Blyth et al., 2021). Historically, their development followed two pathways shaped by the application scale. GCM-oriented LSMs operate on coarse grids (tens to hundreds of kilometers; e.g. Fisher and Koven, 2020) and focus on global water and carbon cycles. By contrast, LSMs used in mesoscale and limited-area models have long used finer resolutions, favoring more accurate landscape representation and parameterizations relevant at kilometer scale over restricted domains or shorter periods, but neglecting groundwater processes (Barlage et al., 2021). Increasing computing power is now blurring this distinction, as GCMs move toward kilometer-scale grid spacing (Segura et al., 2025; Stevens et al., 2019), and mesoscale models increasingly run

https://doi.org/10.5194/egusphere-2026-551
Preprint. Discussion started: 20 March 2026

in climate-mode over large domains and long periods (Lucas-Picher et al., 2021; Schär et al., 2020). This convergence highlights the need for scalable, efficient parameterizations valid across a wide range of environments. Urban land cover exemplifies this challenge: while explicitly represented for decades in mesoscale models (e.g., Masson, 2000), it remains relatively new in GCM-oriented LSMs where coarse grids previously limited its relevance. The shift toward kilometer-scale modeling and rapid urban expansion (Güneralp et al., 2020; Seto et al., 2012), motivate the development of physically based urban schemes in these models. Yet, urban processes are still insufficiently represented in GCM-oriented LSMs despite their strong influence on land–atmosphere (Langendijk et al., 2024; Michau et al., 2025) and land–subsurface interactions (Bhaskar et al., 2016; Oudin et al., 2018).

Urban representations in LSMs began to evolve in the early 2000s, moving from simple to increasingly process-based descriptions. Early approaches treating urban surfaces as natural land covers failed to capture distinct urban radiative, momentum, and heat fluxes at higher spatial resolutions (Lipson et al., 2023). The first step toward explicitly representing cities in LSMs was the introduction of urban bulk schemes, in which grid cell properties such as albedo, roughness length, and surface thermal characteristics were adjusted to reflect urban conditions while still treating the surface as a single homogeneous entity. To improve the representation of the urban energy balance, and to address street scale climate questions, canyon-based models were implemented in LSMs. The Town Energy Budget (TEB; Masson, 2000) implemented an explicit urban canyon geometry within a LSM, distinguishing roofs, walls, and roads and allocating separate energy budgets to each surface. This was followed by multi-layer configurations, such as the Building Effect Parametrization (BEP; Martilli et al., 2002), which added vertical discretization of urban elements and enabled more refined exchanges of heat, momentum, and moisture. The most recent classification of geometries of urban schemes (Lipson et al., 2023) places them on a continuum: (i) non-urban representations (bare soil, vegetation), (ii) one-tile “slab” schemes that aggregate urban surfaces, (iii) two-tile schemes distinguishing between roofs and roads, (iv) canyon-based schemes resolving roofs, walls, and roads separately usually with multi-layers in the canyon, and (v) more complex three-dimensional approaches.

Beyond morphology, urban schemes in LSMs diverge in the processes and fluxes they represent. Comparisons have shown that latent heat flux is often the least well represented, and historically even neglected, under the assumption that vegetation and water availability are minimal in cities (Best and Grimmond, 2015). Over the last decade, however, evidence has emphasized the importance of hydrology and vegetation for correctly simulating latent heat fluxes and model performance during wet conditions, leading to significant advances. Current urban schemes differ in how vegetation is represented: it may be excluded entirely, handled through a sub-tile vegetation fraction with separate energy and water budgets, or integrated directly into the canyon geometry (Krayenhoff et al., 2014; Lemonsu et al., 2012; Redon et al., 2020). Similarly, urban hydrology has progressed from simplified impervious representations (Kusaka et al., 2001; Masson, 2000) to more complete schemes incorporating pervious/impervious distinctions, water reservoirs, irrigation, and subsurface routing (Chancibault et al., 2014; Lemonsu et al., 2007; Oleson et al., 2008; Wouters et al., 2015). Urban hydrology introduces additional challenges

https://doi.org/10.5194/egusphere-2026-551
Preprint. Discussion started: 20 March 2026

due to soil sealing, compaction, preferential flow pathways, and anthropogenic drainage infrastructure. Imperviousness affects both surface and subsurface processes and is not uniquely defined; it may refer to sealed surfaces, hydrologically disconnected areas, or the effective fraction contributing to runoff (Saadi, 2020). These processes influence infiltration, soil moisture, and groundwater recharge, yet remain poorly understood (Bhaskar et al., 2016; Fletcher et al., 2013). This complexity highlights the need for parameterizations in Urban LSMs that explicitly link imperviousness to hydrological properties within the soil column.

The Urban-PLUMBER intercomparison project (Lipson et al., 2023) demonstrated that simpler models, when evaluated as a group, often outperformed more complex ones in simulating local-scale fluxes for large-scale applications such as regional or global climate modeling. The results from the Urban-PLUMBER intercomparison also indicate that model performance is not strictly linked to geometric complexity: schemes that represent hydrology, vegetation, and imperviousness realistically, regardless of whether they are slab, two-tile, or canyon, can perform well across turbulent heat fluxes, whereas complex schemes often underperform when these elements are simplified (Lipson et al., 2023). These findings underscore that accurately representing water availability, imperviousness, and vegetation may be as important as the level of geometric detail.

In its current configuration, the ORCHIDEE land surface model represents urban areas as natural surfaces, more specifically, as bare soil. This simplification limits the model's ability to capture key urban processes, including sensible and latent heat flux partitioning and urban runoff generation. As ORCHIDEE is increasingly applied at fine spatial resolutions, including in convection-permitting coupled simulations below 3 km (Shahi et al., 2022), the absence of an explicit urban representation becomes a critical limitation. ORCHIDEE already includes a detailed and physically based hydrological scheme and a sub-tile vegetation representation through PFTs. However, because urban areas are currently treated as bare soil, ORCHIDEE lacks a mechanism to represent impervious surfaces and to assign surface parameters that reflect urban form and materials.

To reproduce the characteristic signatures of the urban surface energy budget, an urban representation must account for several key surface properties and fluxes that differ markedly from natural areas. First, cities modify the absorbed shortwave radiation by having a lower albedo compared to rural areas because of the materials used in cities and the geometry buildings and streets (Kotopouleas et al., 2021; Qin, 2015). This lower albedo reflects less solar radiation leading to an increase in net radiation (Rnet), and ultimately in higher surface temperatures; The sensible heat is modified by cities buildings, which alter wind speed (depending on the street geometries can either increase or decrease), and increase surface roughness (Sun et al., 2024). The sensible heat is also modified by the different surface temperatures (usually higher than surrounding natural areas) of urban materials which change the temperature gradient between the surface and the air (Barlow, 2014). By reducing the vegetation cover, and by increasing impervious surfaces, cities typically decrease the latent heat flux (Loridan and Grimmond, 2012). This reduction in latent heat, leaves more available energy at the surface to be dissipated as sensible heat. In urban environments, ground heat flux has been estimated to account for 30–40% of net radiation, in contrast to just 10% in rural areas (Rigo and Parlow, 2007). This is the result of the higher thermal capacity and conductivity of urban materials compared

https://doi.org/10.5194/egusphere-2026-551
Preprint. Discussion started: 20 March 2026

to natural areas (Bernabé et al., 2015; Johra, 2021; Wonorahardjo et al., 2020). This refers to what is typically called the storage heat in urban climate studies, with urban materials storing significant heat during the day and releasing it at night (Lindberg et al., 2020). Even if not explored within this manuscript, the anthropogenic heat flux (QF) is a term typically added to urban surface energy budgets. It refers to anthropogenic heat emissions from buildings, from domestic and non-domestic sources (human activities such as heating, cooling, transportation, and industrial processes), with diurnal, seasonal, and regional patterns (Hamilton et al., 2009).

To address the limited representation of urban processes in ORCHIDEE, particularly the effects on energy and water surface budgets, we propose the development of a one-tile urban scheme within the model. This approach builds on advancements in urban parameterizations already implemented in other land surface models. Our goal is to design a scheme that can readily incorporate urban characteristics datasets while remaining computationally efficient. Our objectives are twofold. First, we design an urban one-tile scheme that captures the dominant controls on the urban surface energy and water budgets while remaining consistent with ORCHIDEE's existing structure and computational constraints. We parameterize key urban characteristics (e.g., albedo, thermal conductivity, heat capacity, building height, and impervious surface fraction) such that they can be assigned from global or local urban datasets. Second, we introduce a physically based representation of imperviousness that affects both surface and subsurface hydrological processes. Unlike most one-tile schemes that treat imperviousness as a surface-only property, we allow imperviousness to influence water storage and transfer throughout the soil column by modifying saturated hydraulic conductivity as a function of depth. We evaluate the new scheme at urban and suburban flux tower sites, compare its performance to existing ORCHIDEE configurations, and assess the relative importance of imperviousness-related hydrological processes for urban energy and water fluxes. Section 2 describes the model and the new developments. Section 3 presents the experimental setup and evaluation strategy. Section 4 provides the results, Section 5 discusses their implications, and Section 6 summarizes the conclusions and perspectives.

2 Model Development

2.1 ORganizing Carbon and Hydrology In Dynamic EcosystEms (ORCHIDEE)

ORCHIDEE is the Land Surface Model developed at IPSL (Institut Pierre-Simon Laplace) and used in global and regional climate models, as well as in standalone mode. It simulates coupled water, energy, and carbon fluxes between the land surface and the atmosphere (Boucher et al., 2020; Krinner et al., 2005). This study uses version 2.2 of ORCHIDEE (rev. 8133).

Within each grid cell, land cover is represented as a mosaic of plant functional types (PFTs). The standard configuration includes 15 PFTs: one bare-soil PFT, eight high-vegetation PFTs (forest types), and six low-vegetation PFTs (including grasslands and croplands). Each PFT is associated with its own radiative, morphological, physiological, and phenological characteristics. Hydrological and energy fluxes associated with vegetation (e.g., transpiration, interception, evaporation) are

https://doi.org/10.5194/egusphere-2026-551
Preprint. Discussion started: 20 March 2026

125 computed at the PFT level and are then aggregated to the grid cell scale using a flux-aggregation approach. In contrast, energy fluxes associated with radiative or aerodynamic parameters (e.g., albedo, roughness length) are aggregated as PFT-weighted parameters.

Each grid cell contains three soil columns, one for bare soil, one for high vegetation, and one for low vegetation. This design allows hydrological processes to differ between surface types, for example, in relation to rooting effects. Each soil column is
130 vertically discretized (12 layers, down to a depth of 2 m for hydrology, and 18 m for soil temperature computation), allowing the model to simulate temperature and moisture transfer through the soil profile. For each soil column, ORCHIDEE calculates the surface runoff, and drainage (also called subsurface runoff), representing gravitational outflow at the bottom of the soil column.

2.1.1 Representation of the energy fluxes and surface energy budget

135 The surface energy budget is often described as:

$$R_{net} = H + L_E + G + \frac{dW}{dt}, \quad (1)$$

where Rnet is the net radiation, representing the total balance between incoming shortwave (SW) and longwave (LW) radiation and their respective outgoing components, H is the sensible heat flux, L_E is the latent heat flux, G is the ground heat flux, and dW/dt is the change in heat storage.

140 ORCHIDEE computes these terms following its internal energy budget formulation. Building upon previous Ph.D. thesis and accreditation to supervise research (HDR) thesis (Arboleda-Obando, 2023; Arjdal, 2023; Chéruy, 2018), we summarize here only the components relevant to the development of an urban one-tile scheme. For clarity of presentation, snow-covered conditions and floodplains are not considered in this description. ORCHIDEE computes the energy budget at the grid cell scale. First, the model estimates change in surface temperature based on the downwelling and upwelling radiative terms, and
145 computes R_{net} with the following Equation:

$$R_{net} = (1 - \alpha)\, SW_{in} + \varepsilon\, LW_{in} - \varepsilon\, \sigma\, {T_{surf}}^4 \quad (2)$$

where α is the albedo (unitless); σ is the Stefan–Boltzmann constant ($5.67.10^{-8}$ W m^{-2} K^{-4}); ε is the emissivity (1, unitless); and T_{surf} is the surface temperature (K).

Each vegetation PFT has its own value of albedo (α) , and the value of α for baresoil (α_{MODIS}) is read from MODIS (Moderate
150 Resolution Imaging Spectroradiometer) data (Lurton et al., 2020). This is because the reflectance characteristics of soil vary significantly depending on factors such as composition, moisture, and texture, making it challenging to parameterize bare soil albedo using simple physical models. Unlike vegetation, where albedo can be more homogeneously modeled based on

https://doi.org/10.5194/egusphere-2026-551
Preprint. Discussion started: 20 March 2026

physiological properties, bare soil requires an empirical approach. MODIS satellite data provides precise measurements of these variations, ensuring that local differences in soil reflectance are accurately captured. The resulting albedo of a grid cell is a mean of albedos of bare soil and of the PFTs constituting the grid cell, weighted by the fractional areas of the PFTs of the grid cell (Equation 3).

$$\alpha = f_{PFT_1}\,\alpha_{MODIS} + \sum_{2-15}^{i} f_{PFT_i}\,\alpha_{leaf_i} \tag{3}$$

where f_{PFT_1} is the baresoil fraction of the grid cell; f_{PFT_i} is the PFT_i (vegetation PFTs) fraction of the grid cell; α_{leaf_i} is the albedo of each vegetated PFTs.

For each grid cell at each time step, ORCHIDEE solves the energy budget equations based on a bulk-diffusion approach (Barella-Ortiz et al., 2013). It allows the calculation of the sensible and latent heat fluxes exchanged between the land surface and the atmosphere accounting for the various components of the latent heat flux: soil evaporation, transpiration, snow sublimation. The previously calculated R_{net} from Eq. (2) is redistributed into H, LE, and G, as presented in Eq. (1). The latent and sensible heat fluxes are calculated respectively thanks to Eq. (4) and Eq. (5).

$$H = \rho\, v\, C_d\, c_p\, \left(T_{surf} - T_{air}\right) \tag{4}$$

$$L_E = L_{evap}\, \beta\, \rho\, v\, C_d\, \left(q_{surf} - q_{air}\right) \tag{5}$$

where ρ is air density (kg m^{-3}); v is the horizontal wind speed (m s^{-1}); C_d is the drag coefficient (unitless); c_p is the specific heat capacity of dry air (1004.675 J kg^{-1} K^{-1}); L_{evap} is the latent heat of evaporation or sublimation (2.5008.10^6 or 2.8345.10^6 J kg^{-1}); β is the limiting factor of potential total evapotranspiration (unitless); T_{surf} and T_{air} are the surface and air temperature respectively (K); and q_{surf} and q_{air} are the specific moisture at the surface and in the air (kg kg^{-1}), respectively.

Turbulent transfer of the fluxes between the surface and the atmosphere, is represented thanks to the drag coefficient C_d. The calculation of C_d (also expressed as $1/(r_{ah} \cdot u)$ where u is the wind speed and r_{ah} the aerodynamic resistance) in the standalone version of ORCHIDEE, is calculated with the following equation:

$$C_d = \frac{k^2}{\ln\left(\frac{z_{lev}}{h_{PFT} \cdot z_0}\right)^2} \tag{6}$$

where k is the Von Karman constant; z_{lev} is the height of the first atmospheric layer (10m in standalone simulations); h_{PFT} is the height of the canopy of the considered PFT (fixed) and z_0 is a factor that estimates the roughness height above the canopy and is fixed to 0.0625 (1/16, default value in ORCHIDEE for all PFTs in standalone simulations).

https://doi.org/10.5194/egusphere-2026-551
Preprint. Discussion started: 20 March 2026

Because there is one energy budget per grid cell, the heights need to be converted from the PFT scale to the grid cell scale. After the calculation of all the drag coefficients for each PFT, a mean drag coefficient is calculated thanks to the portion of grid cell occupied by each.

The last term in the decomposition of R_{net} from Eq. (1) is G, the ground heat flux:

$$G = \frac{\lambda}{C_p}\frac{\partial T_{surf}}{\partial z} \tag{7}$$

where λ (W m^{-1} K^{-1}) and C_p (J kg^{-1} K^{-1}) are respectively the soil thermal conductivity and the soil heat capacity, and both vary with soil texture and with the water content of each soil layer.

This expression constitutes the upper boundary condition of the one-dimensional heat diffusion equation used to compute the evolution of soil temperature along the vertical profile. The lower boundary condition is a zero-heat-flux condition at the bottom of the soil column (18 m), following the standard ORCHIDEE configuration. Soil temperature is prognostically calculated by solving the Fourier heat diffusion equation:

$$\frac{\partial T}{\partial t} = \frac{\lambda}{C_p}\frac{\partial^2 T}{\partial z^2} \tag{8}$$

where T is the soil temperature (K).

Finally, the soil thermal properties also change with the presence of water inside the soil layers. Eq. (9) shows the representation of the soil heat capacity as a function of the fraction of water inside the layer. Eq. (10) represents the evolution of soil thermal conductivity as a function of the same fraction:

$$C_p = \left(C_{wet} + 1 - C_{dry}\right) S + C_{dry} \tag{9}$$

$$\lambda = \left(\lambda_S \cdot \lambda_W - \lambda_{dry}\right) S + \lambda_{dry} \tag{10}$$

where, λ_s and λ_w are the heat conductivities for solid soil, and water, respectively; λ_{dry} is the heat conductivity of dry soil (W m^{-1} K^{-1}); S is the total soil saturation degree (m^3 m^{-3}); C_{dry} and C_{wet} are respectively the dry and saturated soil heat capacity (kJ m^{-3} K^{-1}).

https://doi.org/10.5194/egusphere-2026-551
Preprint. Discussion started: 20 March 2026

2.1.2 Representation of water fluxes at the grid cell scale

The description of the computation of the water budget and its different fluxes is detailed in the technical documentation "The hydrol module of ORCHIDEE" (Ducharne et al., 2018), as well as in Ph.D. theses using the ORCHIDEE model (Campoy, 2013; d'Orgeval, 2006). The following sections take up the description of this report and these Ph.D. theses, focusing on the relevant information for the development of an urban one-tile scheme.

The surface water budget reflects the balance between water inputs and outputs at the surface. In ORCHIDEE, it is defined by the partitioning of precipitation into evapotranspiration, surface runoff, drainage, and a change in soil moisture. Each grid cell contains three soil columns for water budget calculations: one for bare soil, one for high vegetation, and one for low vegetation. These columns are 2 m deep and discretized into 12 layers whose thickness increases with depth. The vertical redistribution of soil moisture, here volumetric water content θ ($m^3\ m^{-3}$), in these columns follows a diffusion-based scheme that relies on the Richards equation (De Rosnay et al., 2002), with surface runoff and drainage acting as the upper and lower boundary conditions, respectively and is stated as:

$$\frac{\partial \theta(z,t)}{\partial t} = -\frac{\partial J(z,t)}{\partial z} - s(z,t) \tag{11}$$

where z is depth below the soil surface (m), t is time (s), J is the flux field (m s^{-1}), and s is the sink term ($m^3\ m^{-3}\ s^{-1}$). The flux J follows Darcy's law (Darcy, 1856), later extended to unsaturated soils by Buckingham (1907).

$$J(z,t) = -D\big(\theta(z,t)\big)\frac{\partial \theta(z,t)}{\partial z} + K\big(\theta(z,t)\big) \tag{12}$$

Where $K(\theta)$ and $D(\theta)$ are the hydraulic conductivity and diffusivity (in m s^{-1} and $m^2\ s^{-1}$ respectively). The relationships between K, D, and θ are given by the Mualem (1976) - Van Genuchten (1980) model:

$$K(\theta) = K_s\sqrt{\theta_f}\left(1-\left(1-\theta_f^{1/m}\right)^m\right)^2 \tag{13}$$

$$D(\theta) = \frac{(1-m)K(\theta)}{m\,\mu}\frac{1}{\theta-\theta_r}\theta_f^{-1/m}\left(\theta_f^{1/m}-1\right)^{-m} \tag{14}$$

where K_s is the saturated hydraulic conductivity (m s^{-1}), μ (m^{-1}) corresponds to the inverse of the air entry suction, m is a dimensionless parameter, related to the classical Van Genuchten parameter n, by $m = 1 - 1/n$; θ_r is the residual water content ($m^3\ m^{-3}$), and θ_f the relative humidity ($m^3\ m^{-3}$) defined as $\theta_f = (\theta - \theta_r)/(\theta_s - \theta_r)$, with θ_s the saturated water content ($m^3\ m^{-3}$).

https://doi.org/10.5194/egusphere-2026-551
Preprint. Discussion started: 20 March 2026

In version 2.2 of ORCHIDEE, the vertical profile of saturated hydraulic conductivity $K_s(z)$ is prescribed as a function of depth. Its value at any depth $\boldsymbol{z}$ results from three components:

(i) Reference saturated hydraulic conductivity (K_s^{ref}) at the depth z_{lim} = 0.30m, derived from the dominant USDA soil texture of the grid cell (12-class texture classification). Each grid cell's dominant soil texture influences soil transfer (Ducharne et al., 2018; Tafasca et al., 2020).

(ii) An exponential decrease with depth, controlled by the dimensionless factor $F_K(z)$. This decrease applies from z_{lim} to the bottom of the soil column (2 m).

(iii) A root-induced enhancement in the upper soil layers, represented by a factor $F_{Kroots}(z, c)$, applied only to vegetation soil tiles (c), while bare soil tiles retain a constant K_s over the first 30 cm (d'Orgeval et al., 2008; De Rosnay et al., 2002).

The resulting expression for the saturated hydraulic conductivity profile is:

$$K_s(z) = K_s^{ref}\, F_K(z)\, F_{Kroots}(z, c) \tag{15}$$

where $F_K(z)$ controls the exponential decrease with depth:

$$F_K(z) = \min\left(\max\left(\exp\left(-f(z - z_{lim}), \frac{1}{F_K^{max}}\right), 1\right)\right. \tag{16}$$

Apart from K_s^{ref}, the other three parameters (z_{lim}, f, F_K^{max}) are constants, i.e. they do not depend on the PFT, the soiltile, and the soil texture: f is the decay factor (in m^{-1}); and $F_K(z)$ cannot be smaller than $1/F_K^{max}$. The default values are f = 2 m, and F_K^{max} = 10. f = 2 m, as the soil column depth is 2m, a compromise between representing the vertical distribution of soil moisture realistically while maintaining computational efficiency, with deeper layers contributing less to short-term surface fluxes that are critical for weather and climate modeling. F_K^{max} = 10 as maximum effect of roots is assumed to be at 10 cm depth.

Infiltration is computed using a Green–Ampt type approach. When precipitation exceeds the infiltration capacity at the surface, the non-infiltrated fraction becomes surface runoff (Horton or infiltration-excess runoff). Surface runoff is computed independently for each soil column, and the grid cell runoff is obtained by summing the contributions from the three columns. At the bottom of the 2 m soil column, ORCHIDEE applies a free gravitational drainage boundary condition by default. This means that water leaves the soil whenever hydraulic conductivity at the bottom layer is nonzero. This downward flux is referred to as drainage, or subsurface runoff. As for surface runoff, grid cell drainage is the sum of the drainage from the three soil columns. The total runoff is the sum of drainage and surface runoff. There are no subsurface lateral fluxes between adjacent soil grid cells in the model.

https://doi.org/10.5194/egusphere-2026-551
Preprint. Discussion started: 20 March 2026

In the ORCHIDEE model, evapotranspiration includes evaporation from soil, and vegetation canopy, along with plant transpiration. Evapotranspiration (E_{total}) is the link between the energy balance and the water balance, and can be written as:

$$E_{total} = \beta\, E_{pot} \tag{17}$$

and:

$$E_{pot} = \rho\, v\, C_d \left(q_{surf} - q_{air}\right) \tag{18}$$

The actual evapotranspiration E_{total} is thus calculated from a potential evaporation E_{pot}, and a stress function β_{ET}. This stress function β_{ET} has its own value for each type of evaporation:

$$\beta_{ET} = \frac{A_v\,(\beta_1 + \beta_2) + A_g\,\beta_3}{A_L} \tag{19}$$

where β_1, β_2 and β_3 are the individual stress functions on interception loss, transpiration and bare soil evaporation respectively, and A_v, A_g and A_L are the fractions of vegetated fraction, bare soil fraction, and total land area, respectively. β_1 = 1, since the local evaporation flux from the intercepted water proceeds at its potential rate. The local stress functions β_2 and β_3 are ≤ 1, and all the closer to zero as soil moisture gets limiting.

Once the latent heat flux is calculated with Eq. (5) and Eq. (17), ORCHIDEE calculates the different ET, as:

$$E_{total} = E_{inter} + E_{trans} + E_{soil} \tag{20}$$

with each term depending on the different β previously mentioned, with for instance the E_{soil} being calculated as:

$$E_{soil} = L_{evap}\,\beta_3\,\rho\,\left|\vec{V}\right|\,C_d\,\left(q_{surf} - q_{air}\right) \tag{21}$$

with L_{evap} the latent heat of vaporization.

2.2 New urban parametrization for ORCHIDEE v2.2

2.2.1 Adding an Urban PFT with prescribed albedo and height

The first step in implementing the urban one-tile scheme was to introduce an Urban PFT into ORCHIDEE's land-cover representation. Urban-specific parameter values are prescribed for this PFT. For the energy budget, we assign urban values of albedo, and height of roughness elements. For the water budget, the key parameter is imperviousness, which controls both

https://doi.org/10.5194/egusphere-2026-551
Preprint. Discussion started: 20 March 2026

infiltration and runoff generation. All other PFT attributes remain identical to those of the bare-soil PFT, consistent with the slab-scheme assumption of no vegetation within the urban tile.

In ORCHIDEE, albedo is first computed at the PFT level and then aggregated to the grid cell scale by weighting each PFT contribution by its fractional cover (Eq. 3). For the bare-soil PFT, albedo is prescribed from MODIS, whereas vegetation PFTs use prescribed leaf albedo values ranging from 0.18 to 0.34, depending on vegetation type. For the new Urban PFT, albedo is handled in a flexible manner: it can either be prescribed as a single constant value specified by the user in the simulation namelist or read from an external urban-albedo dataset that ORCHIDEE interpolates onto the model grid. The same structure applies to the parameter controlling effective urban height, which influences aerodynamic roughness and turbulent fluxes. Urban height can correspond to a uniform value defined by the user or be derived from a gridded dataset describing building height or urban morphology. This approach ensures that the urban representation remains compatible with large-scale climate simulations while allowing the use of more detailed datasets when available.

2.2.2 Adding an urban soil column with imperviousness-dependent hydraulic conductivity

In a second step, we introduce a dedicated soil column associated with the Urban PFT, enabling soil water and heat processes to be represented separately from those of bare soil, high vegetation, and low vegetation. Water transfers into the soil depend on several factors, including the saturated hydraulic conductivity K_s (Eqs. 13 and 15). To represent the effects of imperviousness, K_s is reduced to limit water transfer into the soil column. To represent imperviousness within the urban soil column, we modify Eq. (15) by replacing the vegetation root factor $F_{Kroots}(z, c)$ with a constant urban factor K_{fact}^{urban}, which does not depend on depth:

$$K_s(z) = K_s^{ref}\, F_K(z)\, K_{fact}^{urban} \tag{22}$$

When K_{fact}^{urban} equals 1, the original profile of K_s for bare soil remains unmodified. The lowest value assigned to K_{fact}^{urban} is 0.1, as a value of 0 would imply no water transfer within the column, and values lower than 0.1 would result in unrealistically low saturated hydraulic conductivities for certain soil textures (typically with clay). To define the new factor K_{fact}^{urban}, two options are considered. Option "Urban1" considers K_{fact}^{urban} as a constant (same over all urban soil column), while in option "Urban2" K_{fact}^{urban} depends on the imperviousness. The Urban1 option states K_{fact}^{urban} equal to 0.1 to have K_s^{ref} reduced to 10% of its original value:

$$K_{fact}^{urban}{}_1 = 0.1 \tag{23}$$

While the Urban2 option calculates K_{fact}^{urban} as follows:

https://doi.org/10.5194/egusphere-2026-551
Preprint. Discussion started: 20 March 2026

$$K_{fact}^{urban}{}_{2} = \max(1 - 0.9\, f_{imp}, 0.1) \quad (24)$$

where f_{imp} is the value of imperviousness of the urban column and ranges from 0 to 1, so $K_s(z)$ decreases proportionally to f_{imp}. The value of f_{imp} can be specified by the modeler either as a fixed value representative of the urban area under study, e.g., typically 30–60 % (here 0.3-0.6) for medium-density residential areas and 60–80 % (here 0.6-0.8) for high-density residential or mixed-use areas, or by reading from spatially explicit urban imperviousness datasets.

These two options are illustrated in Fig. 1, which represents the saturated hydraulic conductivity for a loam soil over the 2m soil column. The orange line presents the original values from the baresoil column. The purple line presents the saturated hydraulic conductivity for the Urban1 hypothesis. The Urban1 hypothesis is designed to represent a very impervious conceptualization of cities. The pink line presents the saturated hydraulic conductivity for the Urban2 hypothesis, considering an imperviousness equal to 55%.

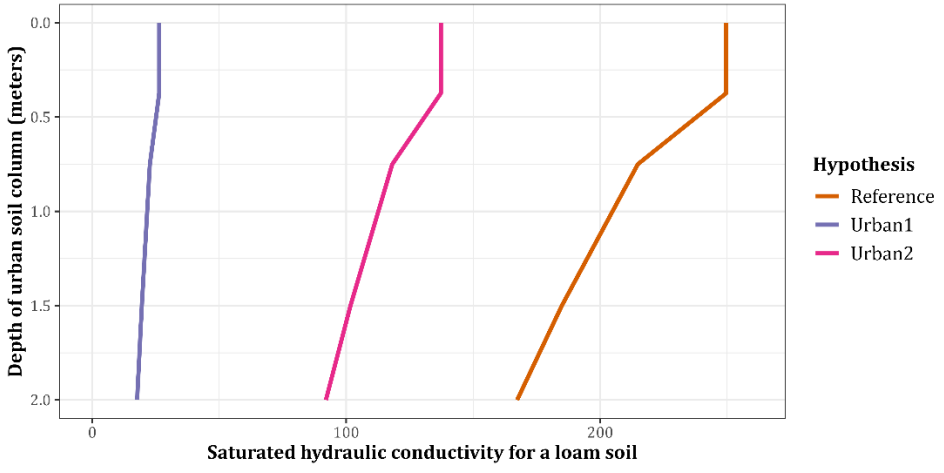

Figure 1: Example profiles of saturated hydraulic conductivity for a reference loam soil (in orange) modified by the two options of imperviousness for an imperviousness equal to 0.55, and a reference saturated hydraulic conductivity of 249.6 mm d^{-1}, values as in Ducharne et al. (2018)

2.2.3 Assigning urban thermal properties to urban-dominated grid cells

The thermal conductivity (λ) and heat capacity (Cp) of the soil are calculated based on soil textures and soil water content (Equations 9 and 10), and are defined at the grid cell scale; they do not depend on PFTs. To take into account the specific urban thermal conductivity and heat capacity, we change the values of λ and Cp for the grid cells where urban areas cover more than 50% of the grid cell. This straightforward binary approach (where the grid cell is assigned either fixed urban values for thermal properties, or retains its initial values) was chosen because these variables are defined at the grid cell scale, rather than at the PFT or soil tile scale. The new prescribed values for urban areas are taken from the NOAH land surface model (He et al., 2023). The thermal conductivity is set to 3.24 W m^{-1} K^{-1} and the heat capacity to 1890 kJ m^{-3} K^{-1}. In comparison, the

https://doi.org/10.5194/egusphere-2026-551
Preprint. Discussion started: 20 March 2026

range of values for grid cells with less than 50% of urban cover is between 0.79 and 2.02 W m^{-1} K^{-1} with a median value of 1.20 W m^{-1} K^{-1} for thermal conductivity, and between 1191 and 2093 kJ m^{-3} K^{-1} with a median value of 1632 kJ m^{-3} K^{-1} for heat capacity. Urban areas therefore exhibit thermal conductivities that exceed those of most other soil textures.

3 Experiments and Methodology

3.1 Experiments

To evaluate the performance of the ORCHIDEE land surface model with the new urban parameterization, including urban albedo, building height, thermal conductivity, heat capacity, and imperviousness, a comprehensive series of 1D standalone simulations is conducted. These simulations are designed to systematically assess the model's sensitivity to these urban parameters in varying climatic and land-use contexts. The simulations are performed across 20 urban flux tower sites (Table 1), sourced from the harmonized gap-filled dataset of Lipson et al. (2022), part of the Urban-PLUMBER project. For each site, the dataset provides all atmospheric forcing variables needed to force a one-dimensional land surface model, as well as site-level information on urban parameters and land use cover. These sites span 13 different countries and encompass a diverse range of climate zones: 11 sites are in temperate climates, 7 in continental climates, 1 in a tropical climate, and 1 in a dry climate. The supplementary data provide a world map of these flux tower sites, including their climates and observed periods (Lipson et al., 2022). Beyond climatic diversity, these urban sites also represent a wide spectrum of land-use characteristics, ranging from highly urbanized areas to low-density urban zones with significant vegetation cover (e.g., trees, grasslands, or croplands). Table 1 also provides a detailed breakdown of site-specific land-use characteristics. The Minneapolis station features two distinct datasets due to differing dominant wind influences, each capturing different land-cover compositions.

The numerical framework consists of multiple simulations for each urban site, each serving a specific purpose in the model evaluation process. The simulations are categorized into benchmark runs and urban parameterization experiments, as outlined in Table 2. The benchmark simulations are the *Baresoil* and the *Lowveget* simulations. *Baresoil* represents the current default urban surface representation in ORCHIDEE, where urban areas are treated as bare soil. The *Lowveget* simulates urban surfaces as the dominant natural land cover (grassland or cropland) in the vicinity, providing a baseline comparison for non-urbanized conditions. Three distinct urban configurations are also tested, all incorporating the newly developed urban albedo, building height, thermal conductivity, and heat capacity parameters. The key difference among them lies in the treatment of imperviousness: *Urban0* which overlooks the influence of imperviousness on K_s to isolate the influence of energy-related parameters; *Urban1* which incorporates the first imperviousness option (Urban1); and *Urban2* which implements the second option (Urban2) for comparative assessment. Further details on grid cell albedo and building height used across all simulations and sites are provided in Supplementary Table S1. These values correspond to the parameter-aggregated approach described for albedo in Eq. (3). For each site, the model is first spun up for 40 years, using repeated cycles of 10 years of meteorological forcing, until soil moisture and temperature reach equilibrium. The subsequent simulation period covers 12–16 years depending on the station (excluding spin-up). Fluxes are computed and saved on a 30-minute time-step.

https://doi.org/10.5194/egusphere-2026-551
Preprint. Discussion started: 20 March 2026

Table 1. Sites description with their sites land use and land cover description (Lipson et al., 2022). Urban, Tree, Low Veget, Bare soil, and Water are expressed in land surface fraction, building height is expressed in meters. Latitude (Lat) and longitude (Lon) are expressed in decimal degrees (°).

Site	City	Country	Observed Period	Lat	Lon	Urban	Tree	Low Veget	Bare soil	Water	Albedo	Building height (m)
AU-Preston	Melbourne	Australia	Aug 2003–Nov 2004	-37.7	145.0	0.62	0.225	0.15	0.005	0	0.151	6.4
AU-SurreyHills	Melbourne	Australia	Feb 2004–Jul 2004	-37.8	145.1	0.54	0.29	0.15	0.01	0.01	0.168	7.2
CA-Sunset	Vancouver	Canada	Jan 2012–Dec 2016	49.2	-123.1	0.68	0.12	0.2	0	0	0.107	4.9
FI-Kumpula	Helsinki	Finland	Dec 2010–Dec 2013	60.2	25.0	0.46	0.3	0.24	0	0	0.142	12.6
FI-Torni	Helsinki	Finland	Dec 2010–Dec 2013	60.2	24.9	0.77	0.15	0.07	0	0.01	0.11	17.9
FR-Capitole	Toulouse	France	Feb 2004–Mar 2005	43.6	1.4	0.9	0.08	0.02	0	0	0.127	15
GR-Heckor	Heraklion	Greece	Jun 2019–Jun 2020	35.3	25.1	0.916	0.04	0.016	0.01	0.019	0.202	11.3
JP-Yoyogi	Tokyo	Japan	Mar 2016–Mar 2020	35.7	139.7	0.92	0.06	0.01	0.01	0	0.133	9
KR-Jungnang	Seoul	South Korea	Jan 2017–Apr 2019	37.6	127.1	0.965	0	0.019	0.016	0	0.12	8.648
KR-Ochang	Ochang	South Korea	Jun 2015–Jul 2017	36.7	127.4	0.47	0.184	0.333	0.013	0	0.166	7.384
MX-Escandon	Mexico City	Mexico	Jun 2011–Sep 2012	19.4	-99.2	0.94	0.06	0	0	0	0.1	9.69
NL-Amsterdam	Amsterdam	Netherlands	Jan 2019–Oct 2020	52.4	4.9	0.68	0.15	0	0	0.17	0.096	14.2
PL-Lipowa	Łódź	Poland	Jan 2008–Dec 2012	51.8	19.4	0.76	0.16	0.08	0	0	0.085	10.2
PL-Narutowicza	Łódź	Poland	Jan 2008–Dec 2012	51.8	19.5	0.65	0.22	0.09	0.04	0	0.087	16
SG-TelokKurau	Singapore	Singapore	Apr 2006–Mar 2007	1.3	103.9	0.85	0.11	0.04	0	0	0.168	9.9
UK-KingsCollege	London	UK	Apr 2012–Jan 2014	51.5	-0.1	0.79	0.03	0.04	0	0.14	0.109	21.3
UK-Swindon	Swindon	UK	May 2011–Apr 2013	51.9	-1.8	0.49	0.09	0.36	0.06	0	0.139	4.5
US-Baltimore	Baltimore	USA	Jan 2002–Jan 2007	39.4	-76.5	0.313	0.536	0.138	0.007	0.006	0.122	5.6
US-Minneapolis1	Minneapolis	USA	Jun 2006–May 2009	45.0	-93.2	0.21	0.38	0.36	0	0.05	0.213	5.05
US-Minneapolis2	Minneapolis	USA	Jun 2006–May 2009	45.0	-93.2	0.05	0.2	0.73	0	0.02	0.213	5.05
US-WestPhoenix	Phoenix	USA	Dec 2011–Jan 2013	33.5	-112.2	0.48	0.05	0.1	0.37	0	0.172	4.5

https://doi.org/10.5194/egusphere-2026-551
Preprint. Discussion started: 20 March 2026

Table 2. Simulations description

Name	PFT 16 is	Albedo	Height	Thermal conductivity	Heat capacity	K_{fact}^{urban}
Low-veget	Low veget (grassland or cropland)	Vegetation value (grassland or cropland)	Vegetation height (grassland or cropland)	Function of soil texture, between 0.79 and 2.02 W m^{-1} K^{-1}	Function of soil texture, between 1191 and 2093 kJ m^{-3} K^{-1}	1
Baresoil	Baresoil (PFT 1)	MODIS	0	Function of soil texture, between 0.79 and 2.02 W m^{-1} K^{-1}	Function of soil texture, between 1191 and 2093 kJ m^{-3} K^{-1}	1
Urban0	Urban	Value from Table 1	Value from Table 1	3.24 W m^{-1} K^{-1} for sites more than 50% urban	1890 kJ m^{-3} K^{-1} for sites more than 50% urban	1
Urban1	Urban	Value from Table 1	Value from Table 1	3.24 W m^{-1} K^{-1} for sites more than 50% urban	1890 kJ m^{-3} K^{-1} for sites more than 50% urban	$K_{fact}^{urban}{}_1$ (Eq. 23)
Urban2	Urban	Value from Table 1	Value from Table 1	3.24 W m^{-1} K^{-1} for sites more than 50% urban	1890 kJ m^{-3} K^{-1} for sites more than 50% urban	$K_{fact}^{urban}{}_2$ (Eq. 24)

3.2 Evaluation strategy

To evaluate the impact of the new urban parameterizations in ORCHIDEE, we compare simulated grid cell averaged fluxes with observed fluxes measured at urban flux tower sites from the Urban-PLUMBER intercomparison (Lipson et al., 2022). Following the Urban-PLUMBER protocol, the AU-Preston site in Melbourne, Australia, is used as a reference station for detailed evaluation (Lipson et al., 2023). In addition to evaluating the diurnal cycle at AU-Preston, we extend the analysis to 20 urban sites spanning a range of climates and urban fractions. For these sites, we analyse the distribution of daily maximum and minimum fluxes across summer and winter seasons to assess the robustness of model behaviour under contrasting energy balance conditions.

Model performance is quantified using two complementary metrics: bias and mean absolute error (MAE). The bias is defined as the mean difference between simulated and observed fluxes (sim – obs), providing information on systematic over- or underestimation. The MAE is defined as the mean of the absolute differences between simulated and observed fluxes, thereby measuring the overall magnitude of deviations regardless of sign. Bias is computed for sensible heat flux (H), latent heat flux (LE), and net radiation (Rnet), and MAE is computed for sensible and latent heat fluxes. Ground heat flux (G) is also analysed in the model outputs, although no observational data are available for evaluation.

https://doi.org/10.5194/egusphere-2026-551
Preprint. Discussion started: 20 March 2026

No additional statistical tests are applied, as the focus is on systematic model–observation differences across multiple years of flux tower data. By comparing results across climates and varying degrees of imperviousness, we assess the consistency of model improvements and identify the conditions under which the new scheme performs best.

4. Results

4.1 Energy budget

Even without the three-dimensional effects of buildings and the source of anthropogenic heat fluxes, urban areas significantly alter the surface energy budget compared to natural landscapes, typically modifying net radiation, increasing nocturnal sensible heat due to building material, and modifying the partitioning between sensible, latent and ground heat fluxes. To assess whether our model developments accurately capture these differences, we first compare simulated fluxes with observations from the AU-Preston station in Melbourne, Australia (Figure 2), the reference site used in both Urban-PLUMBER intercomparisons (Best et al., 2015; Lipson et al., 2023).

The simulations show small differences in net radiation in both summer and winter due to the minimal differences in albedo: 0.141 for *Urban0*, *Urban1*, and *Urban2*, compared to 0.131 for *Lowveget* and 0.110 for *Baresoil*. It is likely that the albedo of bare soil which is read from MODIS already captures some urban albedo information. Urban configurations (*Urban0*, *Urban1*, and *Urban2*) decrease daytime sensible heat flux while enhancing it at night (the curves for the three urban configurations closely overlap in the figure). Also, for the ground heat flux, urban simulations exhibit lower negative daytime values (more heat entering the column) and higher nighttime values (more heat released). More specifically, the *Baresoil* and *Lowveget* simulations produce overlapping curves, and the three urban configurations (*Urban0*, *Urban1*, and *Urban2*) likewise lie nearly on top of each other. These changes in LE, H and G, can be interpreted as a result of increasing heat storage capacity and thermal conductivity of urban surfaces. A higher Cp tends to reduce G, as it increases the amount of energy required to raise the temperature of the soil, leading to slower energy transfer into the ground. However, higher λ increases the rate at which heat is conducted into the ground, thereby increasing G. This increase in G consequently reduces the portion of energy available for sensible and latent heat fluxes at the surface, leading to lower energy partitioning towards atmospheric processes. Additionally, the three urban scenarios exhibit negligible differences, indicating that the representation of imperviousness has limited influence on the energy budget at AU-Preston.

https://doi.org/10.5194/egusphere-2026-551
Preprint. Discussion started: 20 March 2026

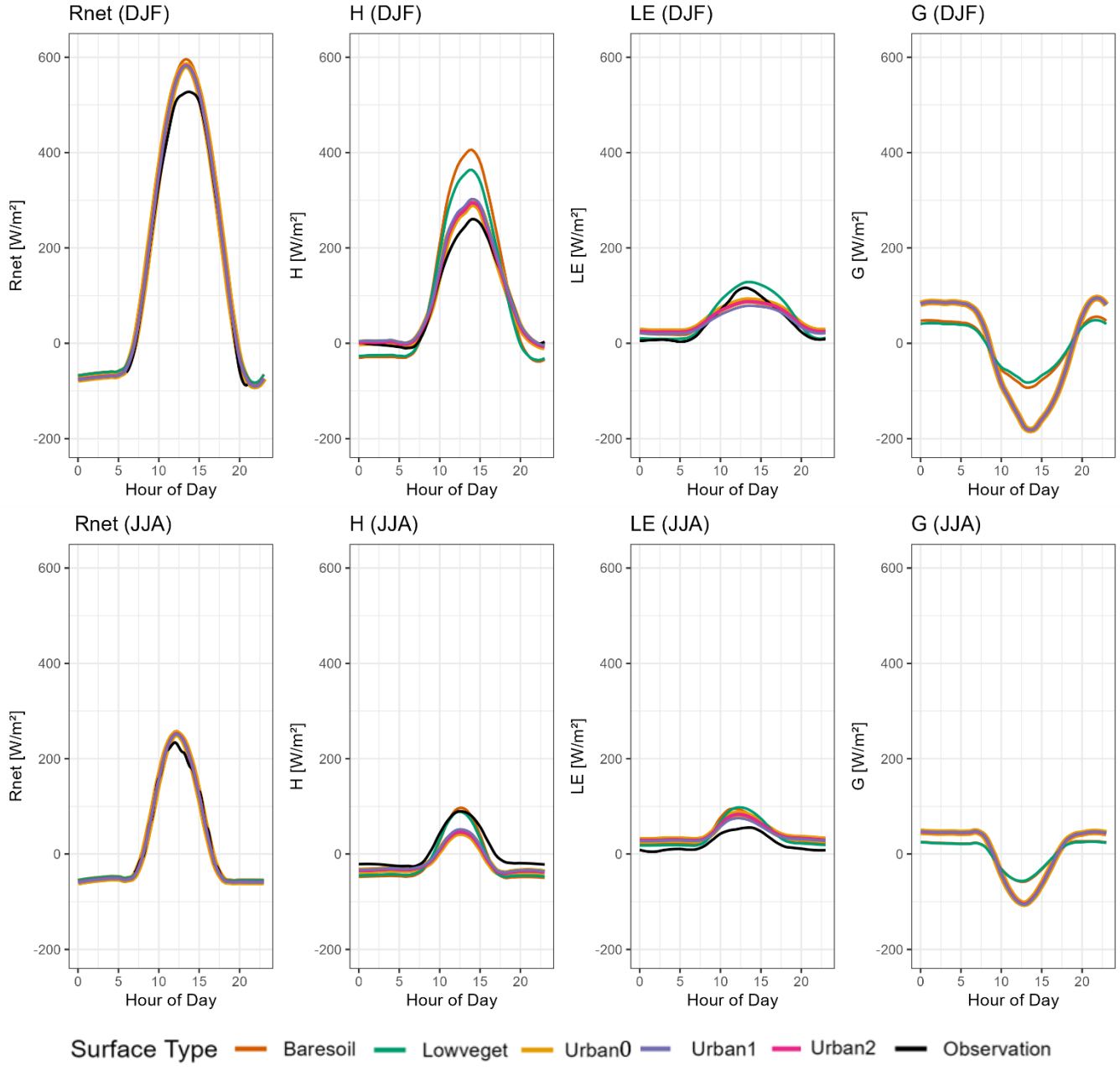

Figure 2: Diurnal cycle of net radiation (Rnet), sensible heat (H), latent heat (LE), and ground heat flux (G) during summer months (DJF – first row), and winter months (JJA – second row) of observational period Aug 2003–Nov 2004 over the station AU-Preston in Melbourne, Australia, the reference station for the Urban-PLUMBER intercomparison projects. The black line represents the observations at the station, while the coloured lines represent the simulations outputs. G is not observed.

When evaluated against the observations, all simulations overestimate Rnet around midday in summer. However, the three urban scenarios (*Urban0*, *Urban1*, and *Urban2*) better reproduce the observed summer sensible heat flux, both at night (close to zero) and during the day. Despite this improvement, they still overestimate daytime sensible heat flux, which is likely related

https://doi.org/10.5194/egusphere-2026-551
Preprint. Discussion started: 20 March 2026

to the overestimation of Rnet. These three urban scenarios still underestimate daytime sensible heat flux in winter, likely because anthropogenic heat fluxes are not represented. Latent heat fluxes are reduced during the day but enhanced at night in urban simulations, with stronger imperviousness further reducing daytime values due to limited water availability. This diurnal contrast arises because, during the day, available energy is high but evaporation is limited by water availability, whereas at night, the release of heat stored in urban materials maintains relatively warm surface temperatures, allowing residual moisture to evaporate, which enhances the latent heat flux compared to natural surfaces. However, this effect is minor compared to other flux modifications. In winter, all simulations overestimate latent heat, though these discrepancies remain small relative to other energy fluxes.

To extend the analysis beyond a single location and assess whether the findings at AU-Preston are representative of broader conditions, we now examine 20 stations spanning different climates and urban covers. This allows us to evaluate whether the sign and magnitude of the model biases identified at AU-Preston (Fig. 2) are consistent across sites. Figure 3 presents the distribution of biases between maximum and minimum daily values of simulated and observed net radiation, sensible heat, and latent heat for winter and summer, two seasons with contrasting surface energy dynamics over the 20 urban sites. This approach highlights model performance during both daytime and nighttime phases of the diurnal cycle.

For maximum daily net radiation, the *Urban* simulations exhibit less bias across the stations, indicating an improvement brought by specifying the observed urban albedo (see supplementary data for grid cell albedo differences across the stations and simulations). In contrast, the *Baresoil* and *Lowveget* simulations show biases with more variability, with an overestimation by *Baresoil* simulations in winter and an underestimation by *Lowveget* simulations in summer.

The different parameterizations used in the model configurations lead to the largest differences for the maximum daily sensible heat flux. In summer, all simulations tend to overestimate sensible heat, the bias exceeding 200 W m^{-2} at some stations. The *Baresoil* and *Lowveget* simulations have a more pronounced overestimation compared to the urban simulations, with the *Baresoil* simulation showing a median bias close to 80 W m^{-2}. In contrast, the *Urban0 and Urban2* simulations have a bias distribution centered closer zero, and 50% of biases between 75 and –45 W m^{-2}. The substantial change in simulated sensible heat is due to increased thermal conductivity in urban simulations, as already seen in Fig. 2. However, many simulations do not match the maximum daily observed sensible heat as closely as for AU-Preston, although the biases are significantly reduced. The *Urban2* simulation introduces only minor changes compared to the *Urban0* simulation for sensible heat. *Urban1*, on the other hand, increases the bias compared to *Urban0* and *Urban2* during summer, but still brings improvement compared to *Baresoil* and *Lowveget*. In winter, the bias distribution shows a different pattern. While *Baresoil* and *Lowveget* simulations have biases in maximum daily sensible heat that are roughly centered around zero, urban simulations exhibit rather a negative bias (less pronounced in *Urban1*), indicating an underestimation of maximum sensible heat. This lower daily sensible heat results from the increased thermal conductivity. The negative bias in *Urban* simulations might be partly explained by the absence of anthropogenic heat fluxes, which are present in the observations but not included in the simulation.

https://doi.org/10.5194/egusphere-2026-551
Preprint. Discussion started: 20 March 2026

Minimum sensible heat flux, which corresponds to the nocturnal sensible heat flux, is generally higher in cities than in natural areas due to the release of stored heat accumulated during the day. As expected, both in winter and summer, *Baresoil* and *Lowveget* simulations exhibit a negative bias, meaning they simulate nocturnal sensible heat that is too low. The *Urban0, Urban1,* and *Urban2* simulations lead to improvements in the simulation of nocturnal sensible heat flux. Furthermore, the *Urban1* simulation, which includes stronger imperviousness, improves further the representation of nocturnal sensible heat during both seasons. Still, *Urban0, Urban1,* and *Urban2* show negative bias minimum sensible heat fluxes in winter, again showing the absence of anthropogenic heat fluxes in the model.

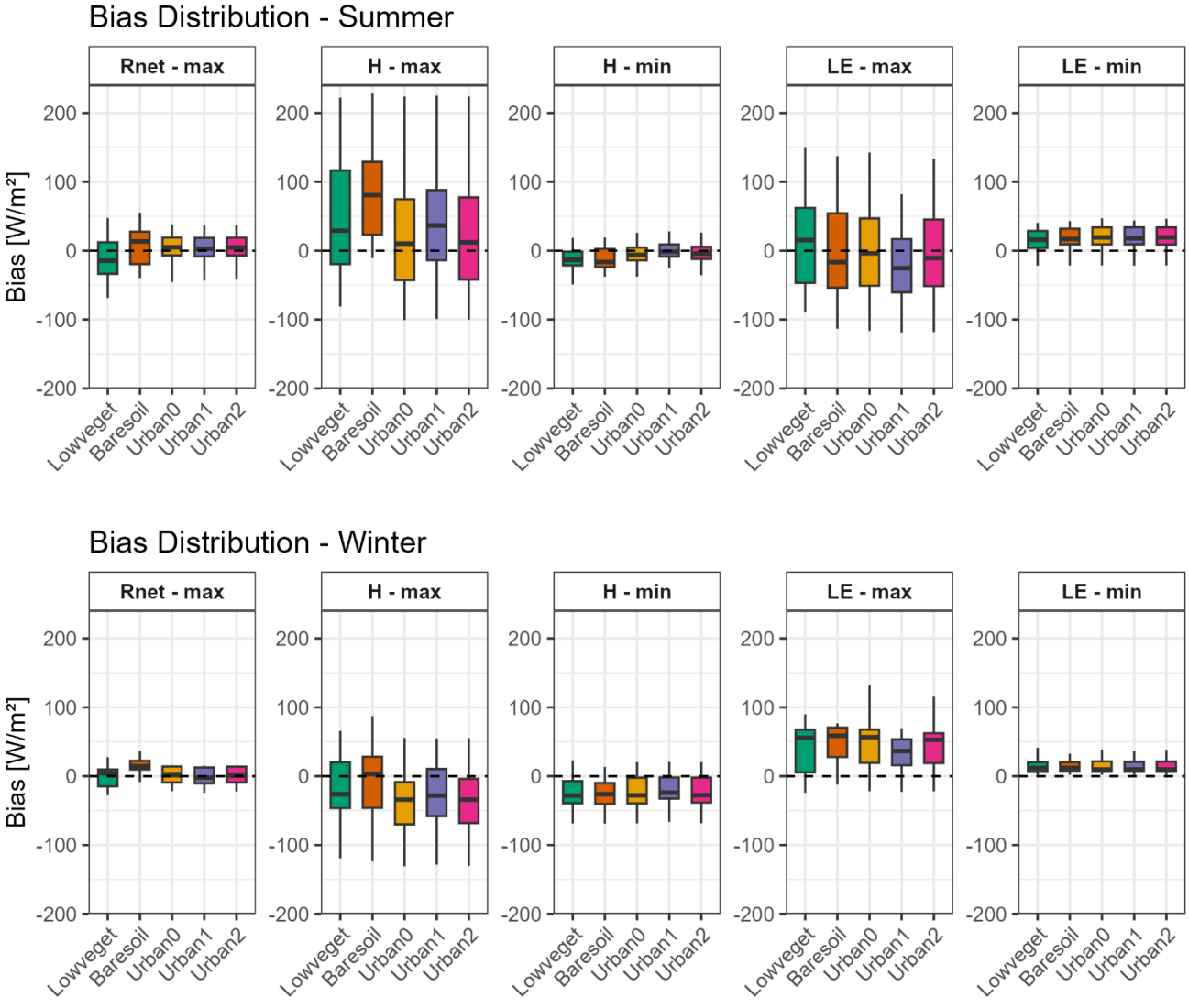

Figure 3: Distribution of mean bias in simulated daily maximum and minimum surface energy fluxes (sensible heat H, latent heat LE, and maximum net radiation Rnet) during summer (first row) and winter (second row) months (DJF/JJA based on hemisphere) across the 20 urban sites.

https://doi.org/10.5194/egusphere-2026-551
Preprint. Discussion started: 20 March 2026

Looking at latent heat, Fig. 3 shows that biases for minimum daily values for both summer and winter are small but consistently positive across all simulations, indicating an overestimation of latent heat flux during the night. Similarly, winter daily latent heat biases are also positive for all simulations, again suggesting an overestimation of latent heat. Still, while *Urban0* and *Urban2* simulation show only small difference in winter maximum latent heat flux bias with the *Baresoil* and *Lowveget* simulations, *Urban1* with its higher imperviousness show some improvement. When focusing on maximum daily latent heat flux during summer, the biases are larger. The distribution of these biases is quite dispersed across the different simulations, indicating an overestimation at some stations and an underestimation at others, likely because local factors such as vegetation or irrigation exert a stronger influence on latent heat fluxes than the choice of urban parameterization alone. As for winter, the *Urban0* and *Urban2* simulations exhibit only small differences to the *Baresoil* simulations, while the *Urban1* simulations, by further reducing water availability for evaporation, decrease the dispersion of bias and rather tend to underestimate summer maximum latent heat flux.

Overall, the Urban configurations improve the representation of simulated surface energy fluxes compared to the *Baresoil* and *Lowveget* configurations, although the magnitude of the improvement varies across variables and seasons. The improvement is substantial for sensible heat in summer, both for daytime maxima and nighttime minima. Improvements in latent heat remain generally small, and the effect of imperviousness is limited, although *Urban1*, with stronger imperviousness provides the most consistent improvement among the three urban configurations. In contrast, the *Urban* configurations do not improve sensible heat in winter, they exhibit a systematic underestimation of maximum sensible heat, consistent with the absence of anthropogenic heat fluxes in the model. Despite this limitation, the urban configurations systematically improve nocturnal sensible heat in both seasons relative to Baresoil and *Lowveget*.

https://doi.org/10.5194/egusphere-2026-551
Preprint. Discussion started: 20 March 2026

4.2 Mean Absolute Errors of latent and sensible heat fluxes over the 20 urban flux towers

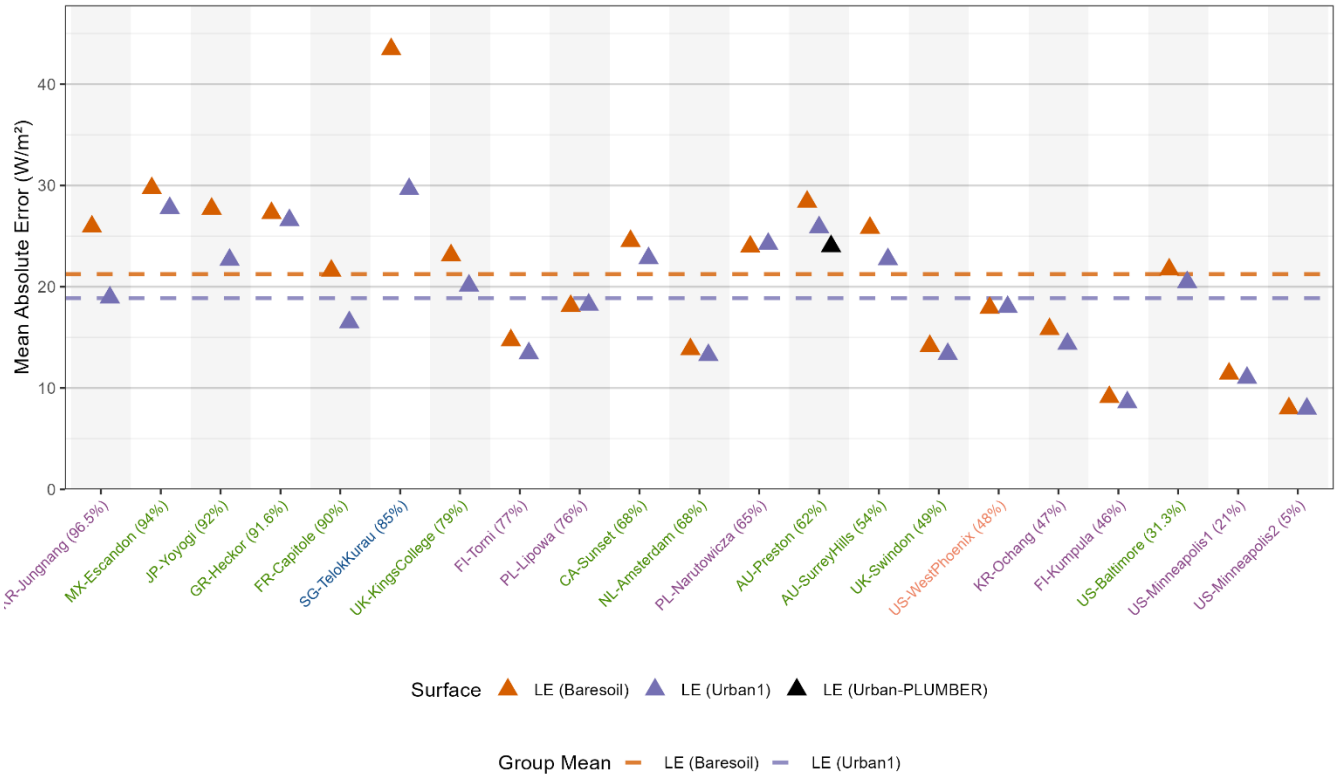

Figure 4: Mean Absolute Error (MAE) of latent heat fluxes (LE) over the 20 urban tower fluxes for the Baresoil and Urban1 simulations. The Urban-PLUMBER value (one black triangle) corresponds to the median Mean Absolute Error of latent heat flux from the "all – detailed" experiment shown in Figure 6 of Lipson et al. (2023). The colours of the station's labels along the x-axis indicate the climate of station: green for Temperate, purple for Continental, orange for Dry, and blue for Tropical. The percentage in these labels indicates the urban fraction around the station. The dashed horizontal lines indicate the mean MAE across all stations, shown in orange for Baresoil and in purple for Urban1.

Following the Urban-PLUMBER intercomparisons (Best et al., 2015; Lipson et al., 2023), we evaluate model performance using the mean absolute error (MAE), which quantifies the average deviation between simulated and observed fluxes. We compare the MAE of the *Baresoil* simulation (representing the original, non-urbanized version of ORCHIDEE) with that of the *Urban1* simulation, which incorporates the new urban parameterizations based on findings from the previous sections. Figures 4 and 5 present the MAE for latent and sensible heat fluxes respectively across the 20 urban flux tower sites for both simulations. On average across all sites, the *Urban1* simulation outperforms the *Baresoil* simulation for both latent heat (by 2.6 W m^{-2}) and sensible heat (by 5.6 W m^{-2}). At the individual station level, *Urban1* improves the MAE for latent heat at all sites. For sensible heat, improvements are also seen at nearly all sites, except for CA-Sunset, UK-Swindon, and FI-Kumpula, where performance is slightly degraded, likely due to an underestimation of daytime sensible heat flux. The new urban developments significantly improve performance at previously poorly performing sites, such as GR-Heckor (−25 W m^{-2}) and FR-Capitole (−14 W m^{-2}) for sensible heat, and SG-TelokKurau (−14 W m^{-2}) for latent heat. However, substantial biases

https://doi.org/10.5194/egusphere-2026-551
Preprint. Discussion started: 20 March 2026

remain at some locations, such as UK-KingsCollege, where sensible heat remains underestimated in both the *Baresoil* and *Urban1* simulations. Including anthropogenic heat fluxes in future model versions may help to address these biases. Figures 4 and 5 also display the mean MAE values for sensible and latent heat from the latest Urban-PLUMBER intercomparison (Lipson et al., 2023) at AU-Preston, representing ensemble model performance using site-specific information. The results show that ORCHIDEE, with the new urban developments, achieves performance comparable to Urban-PLUMBER models, highlighting the relevance and effectiveness of the implemented changes.

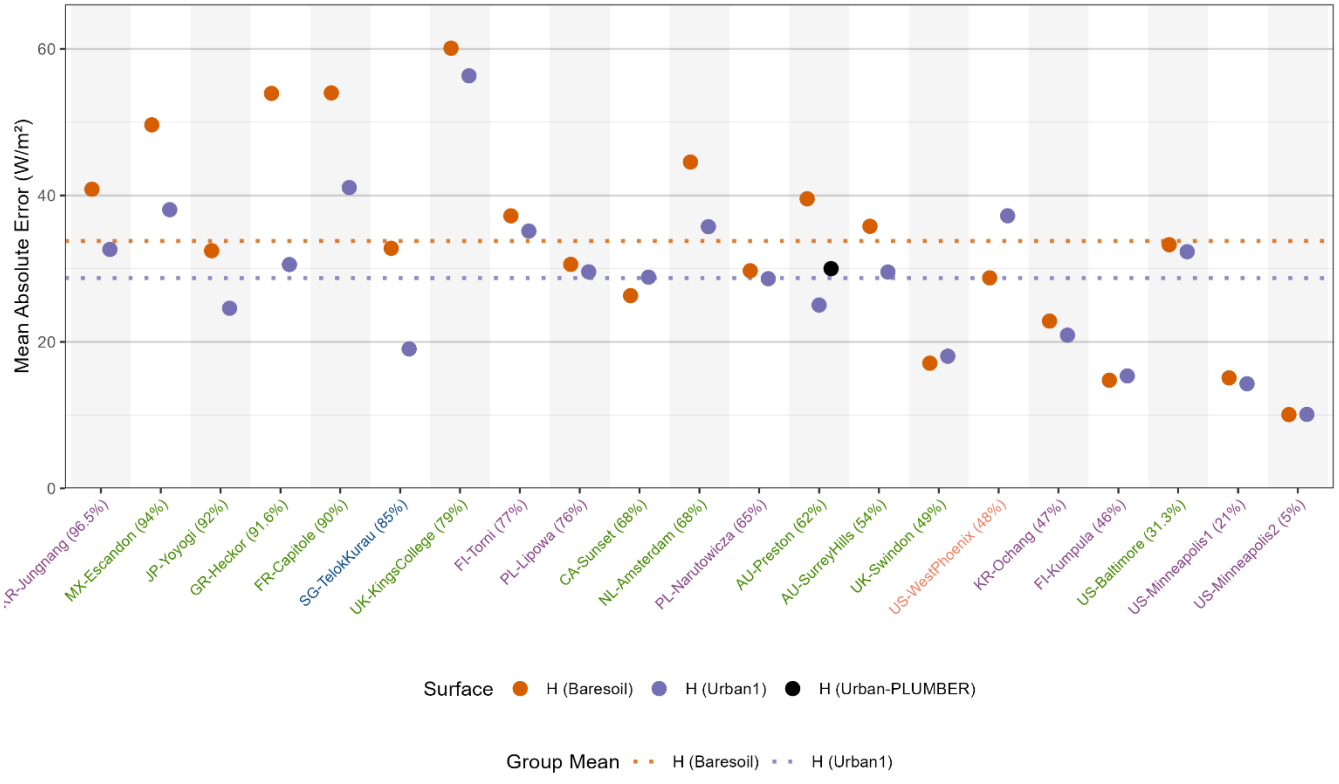

Figure 5: Same as Figure 4, but for the sensible heat fluxes (H).

4.3 Annual water budget

In addition to altering the surface energy budget, urban areas also modify the surface water budget. Most notably, urbanization tends to increase runoff and decrease evapotranspiration, as reflected in the reduced latent heat fluxes discussed in the previous section. While 1D simulations are valuable for comparing simulated fluxes with tower-based flux observations from the Urban-PLUMBER dataset, there are no corresponding observations of soil moisture or runoff available at these stations. Therefore, we limit our analysis to a comparison of the mean annual water budget between the natural surface simulations (*Lowveget* and *Baresoil*) and the *Urban* simulations that include impervious surfaces (*Urban1* and *Urban2*). Figure 6 presents the mean annual water budget across the 20 stations for the four simulations. In addition to climate, initial soil textures and the total amount of

https://doi.org/10.5194/egusphere-2026-551
Preprint. Discussion started: 20 March 2026

annual precipitation (visible in Fig. 6 as the sum of drainage, evapotranspiration, and runoff) and the precipitation characteristics (not visible in Fig. 6, e.g., short intense events vs. long-duration low-intensity rainfall, convective vs. stratiform) also influence differences in the annual water budget between stations. Looking at the natural land cover simulations (*Baresoil* and *Lowveget*), most stations show a water budget dominated by evapotranspiration, except in Canada, where drainage dominates. This is likely due to energy limitations rather than water availability, which constrains evapotranspiration at that site. In the *Urban2* simulation, evapotranspiration is generally not changed compared to the *Baresoil* simulation (+1.1%), but slight increases are observed at some stations (e.g., JP-Yoyogi and FI-Torni), while a decrease is found at the tropical site SG-TelokKurau. The small increases may be linked to enhanced nocturnal latent heat flux, as discussed in the previous section, where redistributed energy from deeper soil column during the night can contribute to evaporation.

The *Urban1* simulation, which includes a higher degree of imperviousness, consistently shows a reduction in evapotranspiration (-7.6%) compared to the *Baresoil* simulation across all stations. However, the dominant changes in the annual water balance introduced by the *Urban* simulations are not related to evapotranspiration, but rather to drainage and runoff. In the natural land cover simulations, drainage exceeds runoff at more than half of the stations (11 out of 20), while the remaining stations (9) show higher runoff than drainage. The *Urban1* simulation, which assumes higher imperviousness, reverses this ratio by significantly reducing drainage and increasing runoff. Only five stations under this scenario still show drainage exceeding runoff. In addition to altering the ratio, *Urban1* doubles the annual runoff at most stations. The *Urban2* simulation, which includes a lower level of imperviousness, also leads to an increase in runoff (with a corresponding decrease in drainage), but the magnitude of change is much smaller. Interestingly, at a few stations (e.g., KR-Ochang and SG-TelokKurau), *Urban2* even shows a slight increase in drainage, suggesting a non-linear response of the water balance to moderate imperviousness. *Urban2* also results in a decrease in runoff at some stations (e.g., FI-Torni and FI-Kumpula). These results suggest that representing saturated hydraulic conductivity as a function of imperviousness yields physically consistent outputs only when conductivity is strongly reduced, as in the *Urban1* hypothesis, but not when the reduction is moderate, as in *Urban2*.

https://doi.org/10.5194/egusphere-2026-551
Preprint. Discussion started: 20 March 2026

Figure 6: Mean annual water budget by station and by simulation. Simulated years depend on station (12-16 years). Titles' colours indicate the climate of station: green for Temperate, purple for Continental, orange for Dry and blue for Tropical. Percentage in title indicates the urban coverage around the station.

5 Discussion

This work represents a first step in integrating urban areas into the ORCHIDEE Land Surface Model. By introducing several key developments, this research has laid the foundation for more accurate urban representation within the model, thereby advancing our ability to simulate urban-climate interactions. In terms of surface energy budgets, the new developments produced the expected outcomes: increased night-time sensible heat flux, decreased day-time sensible heat flux, reduced latent

https://doi.org/10.5194/egusphere-2026-551
Preprint. Discussion started: 20 March 2026

heat flux, and increased ground heat flux with heat released at night, leading to higher night surface temperatures. These changes, together with the reduced biases relative to observations at urban flux-tower sites, confirm that the new urban scheme provides a more realistic representation of turbulent fluxes. In the water budget, the influence on total evapotranspiration and total runoff remains modest; however, the scheme substantially modifies the partitioning between surface runoff and drainage. This shift is particularly important in urban environments, where enhanced surface runoff and reduced subsurface drainage are key drivers of rapid hydrological responses.

Despite the implemented urban developments, the simulations exhibit persistent biases, most notably, an overly strong daily sensible heat flux in summer, an underestimated sensible heat flux in winter during both day and night, and an overestimated latent heat flux during both day and night in summer, and night in winter. These biases should also be considered alongside the inherent uncertainties in flux-tower measurements, which often include some degree of energy-balance non-closure (Mauder et al., 2020). This context helps frame, though does not fully explain, the model–observation differences. Several avenues for improving the one-tile urban scheme developed here emerge thus as clear perspectives. First, the evaluation of ground heat flux (G) revealed strong sensitivity to parameter choices, specifically the thermal conductivity, highlighting G as a key, yet often underrepresented component of the urban surface energy balance. For instance, G was absent from the Urban-PLUMBER harmonized gap-filled datasets for 20 urban flux tower sites used in this study (Lipson et al., 2022b). Our current thermal conductivity value, derived from the NOAH land surface model (He et al., 2023) and relatively high compared to values used in CLM (Lawrence et al., 2019) for instance, may require further refinement. Our current thermal conductivity value (3.24 W m^{-1} K^{-1}), taken from the NOAH land-surface model, is substantially higher than values commonly used in CLM for example, 0.767 W m^{-1} K^{-1} in its original urban implementation (Loridan and Grimmond, 2012) or 1.55 W m^{-1} K^{-1} in the later SURY configuration (Wouters et al., 2016), and may therefore require further refinement. Future work could focus on calibrating thermal conductivity and heat capacity based on observed or region-specific data. While no global database of urban thermal properties was identified during this study, using measured values where available would likely improve realism. Another planned improvement is to update thermal conductivity and heat capacity not only in grid cells where urban cover exceeds a threshold (here 50%), but by applying a weighted average of natural and urban values based on the actual urban fraction. In addition, to improve the sensible heat flux simulation, we also consider incorporating anthropogenic heat fluxes derived from observational datasets when the model is applied at kilometer scale grid spacing.

A more refined representation of urban hydrology could also help address the above biases. While this study introduced a novel physically based approach to model imperviousness, by linking it to saturated hydraulic conductivity and thus allowing it to influence subsurface hydrological processes, several key hydrological behaviors remain unaccounted for. Further development is needed to more fully represent the complexity of urban evapotranspiration, with interception of water for instance. Importantly, advancing the hydrological realism of the model should not be guided by latent heat performance alone, but by a comprehensive evaluation of the full water balance. However, such evaluation is currently limited by a lack of

https://doi.org/10.5194/egusphere-2026-551
Preprint. Discussion started: 20 March 2026

observational data for key hydrological variables (e.g., runoff and soil moisture) at the urban flux tower sites used in this study. This underscores the need for coordinated efforts to collect hydrological data in urban environments to support model development and validation.

The developments presented here were carried out to enable future simulations for which ORCHIDEE, now including an urban representation, is coupled with an atmospheric model to investigate climate–urban interactions. One key perspective of this work is to conduct high-resolution, convection-permitting simulations over Paris to investigate urban effects on temperature, precipitation, and catchment water balance. As ORCHIDEE is used at various spatial resolutions, from coarse to convection-permitting high resolution (<3 km), the development undertaken here is a one-tile scheme which can fit both uses. As highlighted by Zhao et al. (2021), despite the impact of urban areas on climate, most state-of-the-art Earth system models and general circulation models participating in the CMIP do not account for urban regions. This is due to the limited impact of urban areas at coarse resolutions (100-200km). Although constructing multi-model ensembles is considered best practice for providing robust and well-characterized climate projections, relying on non-urban projections for assessing climate-related risks in built environments is inadequate due to their bias regarding urban impacts. To bridge this gap, recent efforts have focused on two approaches: physically downscaling climate projections from one or two GCMs using regional climate models with urban land schemes or directly incorporating urban representation into GCMs. Our development aligns with both approaches. At convection-permitting high resolution, the representation of urban areas becomes even more critical, as cities are explicitly resolved at this scale, and an inaccurate urban energy balance can lead to incorrect atmospheric feedbacks. The CORDEX Flagship Pilot Study URB-RCC is currently investigating how different urban schemes influence simulations of urban temperature and precipitation. Results from the Urban-PLUMBER intercomparison (Lipson et al., 2023) have already shown that performance in resolving the surface energy budget is comparable between one-tile and canyon-type urban schemes. For this reason, the development of a one-tile scheme offers a robust and computationally efficient option for representing urban surfaces in convection-permitting simulations, while remaining scalable for large-scale or global applications. Still, questions related to operational actions such as urban greening, depaving, or planning strategies require insights from more complex schemes that resolve the street canyon, which our urban scheme in ORCHIDEE won't be able to provide.

6 Conclusion

This study presents a first step in implementing urban areas in the ORCHIDEE land surface model. By moving from a baresoil representation of cities to a one-tile urban scheme, we introduce key urban surface properties and propose a novel imperviousness parameterization that links saturated hydraulic conductivity to urban land cover. The new scheme improves the simulation of surface energy fluxes across the 20 urban sites of the Urban-PLUMBER intercomparison project, as reflected by reduced MAE in both latent and sensible heat compared to the baresoil version. Across all stations, mean MAE (mean absolute error) decreases from 21.2 to 18.9 W m^{-2} for latent heat and from 33.8 to 28.7 W m^{-2} for sensible heat. At sites with

https://doi.org/10.5194/egusphere-2026-551
Preprint. Discussion started: 20 March 2026

more than 50% impervious cover, the improvements are even larger, with latent heat decreasing from 24.9 to 21.6 W m^{-2} and sensible heat from 40.5 to 32.5 W m^{-2}. Performance at AU-Preston is consistent with the benchmark range of the Urban-PLUMBER ensemble. For sensible heat, where Urban-PLUMBER mean benchmarks typically achieve MAE between 18.6 and 26.1 W m^{-2}, the original baresoil representation had an MAE of 39.5 W m^{-2}, while the new urban scheme (*Urban1*) reduced it to 25.0 W m^{-2}. For latent heat, where the Urban-PLUMBER mean benchmarks are 18.5–32.9 W m^{-2}, the baresoil scheme produced 28.4 W m^{-2} compared to 25.9 W m^{-2} with the new scheme. In addition, the updated representation modifies local hydrology as expected by increasing runoff and decreasing evapotranspiration. While these developments improve several aspects of urban energy and water balances, some limitations remain. In particular, the simulated reduction in drainage raises questions about the representation of urban recharge, which can be found to increase in observational studies (Bhaskar et al., 2016). The lack of urban runoff or soil moisture observations at the evaluated sites currently limits direct hydrological validation. Future work should address these gaps by running high-resolution 3D simulations at the urban catchment scale, enabling evaluation against streamflow observations. Additional developments, such as spatially and temporally varying urban parameters (e.g., from WUDAPT), refinement of thermal properties, and the inclusion of anthropogenic heat fluxes, will further enhance the performances of this scheme. Together, these improvements will support the use of ORCHIDEE in studying urban climate processes and feedback from city to regional scales.

A perspective of this work is to conduct high-resolution ORCHIDEE simulations over large urban areas with a river routing scheme. These simulations would allow the evaluation of the urban module in which urban parameters such as albedo, building height, and imperviousness can vary both spatially and temporally. In the present 1D experiments, these parameters were prescribed for each site. However, the scheme developed here is capable of reading and interpolating urban data maps (e.g., LCZ maps or datasets describing imperviousness, albedo, and building heights), although this functionality was not demonstrated in the 1D framework. Using spatially distributed inputs would enable the model to take advantage of, and remain consistent with, comprehensive urban datasets such as the WUDAPT database (Ching et al., 2018). Including urban catchments within the simulation domain would also create opportunities to evaluate the model developments against streamflow measurements, which are generally more available than runoff or soil moisture observations. Further consideration could be given to whether additional processes, such as subsurface water lateral fluxes should be included in high-resolution climate simulations to assess urban water resources.

Code and data availability

The initial version of the ORCHIDEE LSM used for this study corresponds to tag 2.2, revision 8133 and is freely available from https://forge.ipsl.jussieu.fr/orchidee/log/branches/ORCHIDEE_2_2/. It is provided under a CeCILL-C license (French equivalent to the LGPL license). The version of the ORCHIDEE LSM with the urban developments described in this paper is archived on Zenodo (Lalonde et al., 2026c) and is available at https://doi.org/10.5281/zenodo.18413342. Atmospheric forcing

https://doi.org/10.5194/egusphere-2026-551
Preprint. Discussion started: 20 March 2026

data and observations (Data for "Harmonized gap-filled dataset from 20 urban flux tower sites" for the Urban-PLUMBER project) are available at https://zenodo.org/records/7104984 (Lipson et al., 2022a). The simulation outputs are available at https://doi.org/10.5281/zenodo.19075902 (Lalonde et al., 2026a). The scripts to process the data and plot the figures are available at https://doi.org/10.5281/zenodo.19097389 (Lalonde et al., 2026b).

Acknowledgements

We gratefully acknowledge the support of the LEFE program from INSU/CNRS, of EUR IPSL and Graduate School "Géosciences, Climat, Environnement, Planètes" of Université Paris-Saclay for contributing to the funding of this research. We also thank the ESPRI mesocenter of IPSL for providing computational resources and data access. We thank Lluis Fita, Jan Polcher, and Romain Pennel for their insightful discussions on the ORCHIDEE model.

Competing interests

The authors declare that they have no conflict of interest.

References

Arboleda-Obando, P.F., 2023. Feedback from groundwater and irrigation on past and future climate simulated by the IPSL climate model (Ph.D.). Sorbonne Université, Paris, france.

Arjdal, K., 2023. Modeling the surface-atmosphere coupling in the Moroccan semi-arid plains in the context of climate change (Ph.D.). Institut Polytechnique de Paris et Université Mohammed VI Polytechnique, Benguerir, Marocco.

Barella-Ortiz, A., Polcher, J., Tuzet, A., Laval, K., 2013. Potential evaporation estimation through an unstressed surface-energy balance and its sensitivity to climate change. Hydrology and Earth System Sciences 17, 4625–4639. https://doi.org/10.5194/hess-17-4625-2013

Barlage, M., Chen, F., Rasmussen, R., Zhang, Z., Miguez-Macho, G., 2021. The Importance of Scale-Dependent Groundwater Processes in Land-Atmosphere Interactions Over the Central United States. Geophysical Research Letters 48, e2020GL092171. https://doi.org/10.1029/2020GL092171

Barlow, J.F., 2014. Progress in observing and modelling the urban boundary layer. Urban Climate, ICUC8: The 8th International Conference on Urban Climate and the 10th Symposium on the Urban Environment 10, 216–240. https://doi.org/10.1016/j.uclim.2014.03.011

Bernabé, A., Bernard, J., Musy, M., Andrieu, H., Bocher, E., Calmet, I., Kéravec, P., Rosant, J.-M., 2015. Radiative and heat storage properties of the urban fabric derived from analysis of surface forms. Urban Climate 12, 205–218. https://doi.org/10.1016/j.uclim.2015.04.001

Best, M.J., Abramowitz, G., Johnson, H.R., Pitman, A.J., Balsamo, G., Boone, A., Cuntz, M., Decharme, B., Dirmeyer, P.A., Dong, J., Ek, M., Guo, Z., Haverd, V., Van Den Hurk, B.J.J., Nearing, G.S., Pak, B., Peters-Lidard, C., Santanello, J.A., Stevens, L., Vuichard, N., 2015. The Plumbing of Land Surface Models: Benchmarking Model Performance. Journal of Hydrometeorology 16, 1425–1442. https://doi.org/10.1175/JHM-D-14-0158.1

Best, M.J., Grimmond, C.S.B., 2015. Key Conclusions of the First International Urban Land Surface Model Comparison Project. Bulletin of the American Meteorological Society 96, 805–819. https://doi.org/10.1175/BAMS-D-14-00122.1

Bhaskar, A.S., Beesley, L., Burns, M.J., Fletcher, T.D., Hamel, P., Oldham, C.E., Roy, A.H., 2016. Will it rise or will it fall? Managing the complex effects of urbanization on base flow. Freshwater Science 35, 293–310. https://doi.org/10.1086/685084

https://doi.org/10.5194/egusphere-2026-551
Preprint. Discussion started: 20 March 2026

Blyth, E.M., Arora, V.K., Clark, D.B., Dadson, S.J., De Kauwe, M.G., Lawrence, D.M., Melton, J.R., Pongratz, J., Turton, R.H., Yoshimura, K., Yuan, H., 2021. Advances in Land Surface Modelling. Curr Clim Change Rep 7, 45–71. https://doi.org/10.1007/s40641-021-00171-5

Boucher, O., Servonnat, J., Albright, A.L., Aumont, O., Balkanski, Y., Bastrikov, V., Bekki, S., Bonnet, R., Bony, S., Bopp, L., Braconnot, P., Brockmann, P., Cadule, P., Caubel, A., Cheruy, F., Codron, F., Cozic, A., Cugnet, D., D'Andrea, F., Davini, P., De Lavergne, C., Denvil, S., Deshayes, J., Devilliers, M., Ducharne, A., Dufresne, J., Dupont, E., Éthé, C., Fairhead, L., Falletti, L., Flavoni, S., Foujols, M., Gardoll, S., Gastineau, G., Ghattas, J., Grandpeix, J., Guenet, B., Guez, L., E., Guilyardi, E., Guimberteau, M., Hauglustaine, D., Hourdin, F., Idelkadi, A., Joussaume, S., Kageyama, M., Khodri, M., Krinner, G., Lebas, N., Levavasseur, G., Lévy, C., Li, L., Lott, F., Lurton, T., Luyssaert, S., Madec, G., Madeleine, J., Maignan, F., Marchand, M., Marti, O., Mellul, L., Meurdesoif, Y., Mignot, J., Musat, I., Ottlé, C., Peylin, P., Planton, Y., Polcher, J., Rio, C., Rochetin, N., Rousset, C., Sepulchre, P., Sima, A., Swingedouw, D., Thiéblemont, R., Traore, A.K., Vancoppenolle, M., Vial, J., Vialard, J., Viovy, N., Vuichard, N., 2020. Presentation and Evaluation of the IPSL-CM6A-LR Climate Model. J Adv Model Earth Syst 12, e2019MS002010. https://doi.org/10.1029/2019MS002010

Buckingham, E., 1907. Studies on the movement of soil moisture. US Dept. Agic. Bur. Soils Bull. 38.

Campoy, A., 2013. Influence de l'hydrologie souterraine sur la modélisation du climat à l'échelle régionale et globale (Ph.D.). Université Pierre et Marie Curie, Paris, france.

Chancibault, K., Lemonsu, A., Brun, J.-M., Munck, C.D., Allard, A., Long, N., Bellec, A., Masson, V., 2014. Hydrological Evaluation of Urban Greening Scenarios: Application to the City of Nantes, France.

Chéruy, F., 2018. Etude par modélisation des interactions surface-atmosphère à l'échelle globale (HDR). Sorbonne Université, Paris, france.

Ching, J., Mills, G., Bechtel, B., See, L., Feddema, J., Wang, X., Ren, C., Brousse, O., Martilli, A., Neophytou, M., Mouzourides, P., Stewart, I., Hanna, A., Ng, E., Foley, M., Alexander, P., Aliaga, D., Niyogi, D., Shreevastava, A., Bhalachandran, P., Masson, V., Hidalgo, J., Fung, J., Andrade, M., Baklanov, A., Dai, W., Milcinski, G., Demuzere, M., Brunsell, N., Pesaresi, M., Miao, S., Mu, Q., Chen, F., Theeuwes, N., 2018. WUDAPT: An Urban Weather, Climate, and Environmental Modeling Infrastructure for the Anthropocene. Bulletin of the American Meteorological Society 99, 1907–1924. https://doi.org/10.1175/BAMS-D-16-0236.1

d'Orgeval, T., 2006. Impact du changement climatique sur le cycle de l'eau en Afrique de l'Ouest : modélisation et incertitudes. (Ph.D.). Université Pierre et Marie Curie, Paris, france.

d'Orgeval, T., Polcher, J., De Rosnay, P., 2008. Sensitivity of the West African hydrological cycle in ORCHIDEE to infiltration processes. Hydrology and Earth System Sciences 12, 1387–1401. https://doi.org/www.hydrol-earth-syst-sci.net/12/1387/2008/

Darcy, H., 1856. Les fontaines publiques de la ville de Dijon: exposition et application des principes à suivre et des formules à employer dans les questions de distribution d'eau, Victor dalmont. ed.

De Rosnay, P., Polcher, J., Bruen, M., Laval, K., 2002. Impact of a physically based soil water flow and soil-plant interaction representation for modeling large-scale land surface processes. J. Geophys. Res. 107. https://doi.org/10.1029/2001JD000634

Ducharne, A., Maignan, F., Vuichard, N., Ghattas, J., Wang, F., Peylin, P., Polcher, J., Guimberteau, M., Maugis, P., Tafasca, S., Tootchi, A., Verhoef, A., Mizuochi, H., 2018. The hydrol module of ORCHIDEE: scientific documentation.

Fisher, R.A., Koven, C.D., 2020. Perspectives on the Future of Land Surface Models and the Challenges of Representing Complex Terrestrial Systems. Journal of Advances in Modeling Earth Systems 12, e2018MS001453. https://doi.org/10.1029/2018MS001453

Fletcher, T.D., Andrieu, H., Hamel, P., 2013. Understanding, management and modelling of urban hydrology and its consequences for receiving waters: A state of the art. Advances in Water Resources 51, 261–279. https://doi.org/10.1016/j.advwatres.2012.09.001

Güneralp, B., Reba, M., Hales, B.U., Wentz, E.A., Seto, K.C., 2020. Trends in urban land expansion, density, and land transitions from 1970 to 2010: a global synthesis. Environ. Res. Lett. 15, 044015. https://doi.org/10.1088/1748-9326/ab6669

https://doi.org/10.5194/egusphere-2026-551
Preprint. Discussion started: 20 March 2026

Hamilton, I.G., Davies, M., Steadman, P., Stone, A., Ridley, I., Evans, S., 2009. The significance of the anthropogenic heat emissions of London's buildings: A comparison against captured shortwave solar radiation. Building and Environment 44, 807–817. https://doi.org/10.1016/j.buildenv.2008.05.024

He, C., Valayamkunnath, P., Barlage, M., Chen, F., Gochis, D., Cabell, R., Schneider, T., Rasmussen, R., Niu, G.-Y., Yang, Z.-L., Niyogi, D., Ek, M., 2023. The Community Noah-MP Land Surface Modeling System Technical Description Version 5.0. NCAR/UCAR. https://doi.org/10.5065/EW8G-YR95

Johra, H., 2021. Thermal properties of building materials - Review and database. Department of the Built Environment, Aalborg University. https://doi.org/10.54337/aau456230861

Kotopouleas, A., Giridharan, R., Nikolopoulou, M., Watkins, R., Yeninarcilar, M., 2021. Experimental investigation of the impact of urban fabric on canyon albedo using a 1:10 scaled physical model. Solar Energy 230, 449–461. https://doi.org/10.1016/j.solener.2021.09.074

Krayenhoff, E.S., Christen, A., Martilli, A., Oke, T.R., 2014. A Multi-layer Radiation Model for Urban Neighbourhoods with Trees. Boundary-Layer Meteorol 151, 139–178. https://doi.org/10.1007/s10546-013-9883-1

Krinner, G., Viovy, N., de Noblet-Ducoudré, N., Ogée, J., Polcher, J., Friedlingstein, P., Ciais, P., Sitch, S., Prentice, I.C., 2005. A dynamic global vegetation model for studies of the coupled atmosphere-biosphere system. Global Biogeochem. Cycles 19. https://doi.org/10.1029/2003GB002199

Kusaka, H., Kondo, H., Kikegawa, Y., Kimura, F., 2001. A Simple Single-Layer Urban Canopy Model For Atmospheric Models: Comparison With Multi-Layer And Slab Models. Boundary-Layer Meteorology 101, 329–358. https://doi.org/10.1023/A:1019207923078

Lalonde, M., Bastin, S., Oudin, L., Arboleda Obando, P.F., Ducharne, A., 2026a. Simulations - Benchmarking and evaluating a new urban scheme in the ORCHIDEE land surface model. https://doi.org/10.5281/zenodo.19075902

Lalonde, M., Bastin, S., Oudin, L., Arboleda Obando, P.F., Ducharne, A., 2026b. Scripts - Benchmarking and evaluating a new urban scheme in the ORCHIDEE land surface model. https://doi.org/10.5281/zenodo.19097389

Lalonde, M., Bastin, S., Oudin, L., Arboleda-Obando, P., Ducharne, A., 2026c. Source Code - Benchmarking and evaluating a new urban scheme in the ORCHIDEE land surface model. https://doi.org/10.5281/zenodo.18413342

Langendijk, G.S., Halenka, T., Hoffmann, P., Adinolfi, M., Aldama Campino, A., Asselin, O., Bastin, S., Bechtel, B., Belda, M., Bushenkova, A., Campanale, A., Chun, K.P., Constantinidou, K., Coppola, E., Demuzere, M., Doan, Q.-V., Evans, J., Feldmann, H., Fernandez, J., Fita, L., Hadjinicolaou, P., Hamdi, R., Hundhausen, M., Grawe, D., Johannsen, F., Milovac, J., Katragkou, E., Kerroumi, N.E.I., Kotlarski, S., Le Roy, B., Lemonsu, A., Lennard, C., Lipson, M., Mandal, S., Muñoz Pabón, L.E., Pavlidis, V., Pietikäinen, J.-P., Raffa, M., Raluy-López, E., Rechid, D., Ito, R., Schulz, J.-P., Soares, P.M.M., Takane, Y., Teichmann, C., Thatcher, M., Top, S., Van Schaeybroeck, B., Wang, F., Yuan, J., 2024. Towards better understanding the urban environment and its interactions with regional climate change - The WCRP CORDEX Flagship Pilot Study URB-RCC. Urban Climate 58, 102165. https://doi.org/10.1016/j.uclim.2024.102165

Lawrence, D.M., Fisher, R.A., Koven, C.D., Oleson, K.W., Swenson, S.C., Bonan, G., Collier, N., Ghimire, B., Van Kampenhout, L., Kennedy, D., Kluzek, E., Lawrence, P.J., Li, F., Li, H., Lombardozzi, D., Riley, W.J., Sacks, W.J., Shi, M., Vertenstein, M., Wieder, W.R., Xu, C., Ali, A.A., Badger, A.M., Bisht, G., Van Den Broeke, M., Brunke, M.A., Burns, S.P., Buzan, J., Clark, M., Craig, A., Dahlin, K., Drewniak, B., Fisher, J.B., Flanner, M., Fox, A.M., Gentine, P., Hoffman, F., Keppel-Aleks, G., Knox, R., Kumar, S., Lenaerts, J., Leung, L.R., Lipscomb, W.H., Lu, Y., Pandey, A., Pelletier, J.D., Perket, J., Randerson, J.T., Ricciuto, D.M., Sanderson, B.M., Slater, A., Subin, Z.M., Tang, J., Thomas, R.Q., Val Martin, M., Zeng, X., 2019. The Community Land Model Version 5: Description of New Features, Benchmarking, and Impact of Forcing Uncertainty. J Adv Model Earth Syst 11, 4245–4287. https://doi.org/10.1029/2018MS001583

Lemonsu, A., Masson, V., Berthier, E., 2007. Improvement of the hydrological component of an urban soil–vegetation–atmosphere–transfer model. Hydrological Processes 21, 2100–2111. https://doi.org/10.1002/hyp.6373

Lemonsu, A., Masson, V., Shashua-Bar, L., Erell, E., Pearlmutter, D., 2012. Inclusion of vegetation in the Town Energy Balance model for modelling urban green areas. Geosci. Model Dev. 5, 1377–1393. https://doi.org/10.5194/gmd-5-1377-2012

https://doi.org/10.5194/egusphere-2026-551
Preprint. Discussion started: 20 March 2026

Lindberg, F., Olofson, K.F.G., Sun, T., Grimmond, C.S.B., Feigenwinter, C., 2020. Urban storage heat flux variability explored using satellite, meteorological and geodata. Theor Appl Climatol 141, 271–284. https://doi.org/10.1007/s00704-020-03189-1

Lipson, M., Grimmond, S., Best, M., Chow, W., Christen, A., Chrysoulakis, N., Coutts, A., Crawford, B., Earl, S., Evans, J., Fortuniak, K., Heusinkveld, B.G., Hong, J.-W., Hong, J., Järvi, L., Jo, S., Kim, Y.-H., Kotthaus, S., Lee, K., Masson, V., McFadden, J.P., Michels, O., Pawlak, W., Roth, M., Sugawara, H., Tapper, N., Velasco, E., Ward, H.C., 2022a. Data for "Harmonized gap-filled dataset from 20 urban flux tower sites" for the Urban-PLUMBER project. https://doi.org/10.5281/zenodo.7104984

Lipson, M., Grimmond, S., Best, M., Chow, W.T.L., Christen, A., Chrysoulakis, N., Coutts, A., Crawford, B., Earl, S., Evans, J., Fortuniak, K., Heusinkveld, B.G., Hong, J.-W., Hong, J., Järvi, L., Jo, S., Kim, Y.-H., Kotthaus, S., Lee, K., Masson, V., McFadden, J.P., Michels, O., Pawlak, W., Roth, M., Sugawara, H., Tapper, N., Velasco, E., Ward, H.C., 2022b. Harmonized gap-filled datasets from 20 urban flux tower sites. Earth Syst. Sci. Data 14, 5157–5178. https://doi.org/10.5194/essd-14-5157-2022

Lipson, M.J., Grimmond, S., Best, M., Abramowitz, G., Coutts, A., Tapper, N., Baik, J.-J., Beyers, M., Blunn, L., Bousseta, S., Bou-Zeid, E., De Kauwe, M.G., De Munck, C., Demuzere, M., Fatichi, S., Fortuniak, K., Han, B.-S., Hendry, M.A., Kikegawa, Y., Kondo, H., Lee, D.-I., Lee, S.-H., Lemonsu, A., Machado, T., Manoli, G., Martilli, A., Masson, V., McNorton, J., Meili, N., Meyer, D., Nice, K.A., Oleson, K.W., Park, S.-B., Roth, M., Schoetter, R., Simón-Moral, A., Steeneveld, G.-J., Sun, T., Takane, Y., Thatcher, M., Tsiringakis, A., Varentsov, M., Wang, C., Wang, Z.-H., Pitman, A.J., 2023. Evaluation of 30 urban land surface models in the Urban-PLUMBER project: Phase 1 results. Quarterly Journal of the Royal Meteorological Society 150, 126–169. https://doi.org/10.1002/qj.4589

Loridan, T., Grimmond, C.S.B., 2012. Characterization of Energy Flux Partitioning in Urban Environments: Links with Surface Seasonal Properties. Journal of Applied Meteorology and Climatology 51, 219–241. https://doi.org/10.1175/JAMC-D-11-038.1

Lucas-Picher, P., Argüeso, D., Brisson, E., Tramblay, Y., Berg, P., Lemonsu, A., Kotlarski, S., Caillaud, C., 2021. Convection-permitting modeling with regional climate models: Latest developments and next steps. WIREs Climate Change 12, e731. https://doi.org/10.1002/wcc.731

Lurton, T., Balkanski, Y., Bastrikov, V., Bekki, S., Bopp, L., Braconnot, P., Brockmann, P., Cadule, P., Contoux, C., Cozic, A., Cugnet, D., Dufresne, J.-L., Éthé, C., Foujols, M.-A., Ghattas, J., Hauglustaine, D., Hu, R.-M., Kageyama, M., Khodri, M., Lebas, N., Levavasseur, G., Marchand, M., Ottlé, C., Peylin, P., Sima, A., Szopa, S., Thiéblemont, R., Vuichard, N., Boucher, O., 2020. Implementation of the CMIP6 Forcing Data in the IPSL-CM6A-LR Model. Journal of Advances in Modeling Earth Systems 12, e2019MS001940. https://doi.org/10.1029/2019MS001940

Martilli, A., Clappier, A., Rotach, M.W., 2002. An Urban Surface Exchange Parameterisation for Mesoscale Models. Boundary-Layer Meteorology 104, 261–304. https://doi.org/10.1023/A:1016099921195

Masson, V., 2000. A Physically-Based Scheme For The Urban Energy Budget In Atmospheric Models. Boundary-Layer Meteorology 94, 357–397. https://doi.org/10.1023/A:1002463829265

Mauder, M., Foken, T., Cuxart, J., 2020. Surface-Energy-Balance Closure over Land: A Review. Boundary-Layer Meteorol 177, 395–426. https://doi.org/10.1007/s10546-020-00529-6

Michau, Y., Lemonsu, A., Lucas-Picher, P., Bastin, S., Caillaud, C., de Vries, H., Adinolfi, M., Raffa, M., Katragkou, E., Coppola, E., 2025. Projected evolution of the Urban climate and heatwaves using an ensemble of convection-permitting regional climate models. Climatic Change 178, 154. https://doi.org/10.1007/s10584-025-03990-9

Mualem, Y., 1976. A new model for predicting the hydraulic conductivity of unsaturated porous media. Water Resources Research 12, 513–522. https://doi.org/10.1029/WR012i003p00513

Oleson, K., Bonan, G.B., Feddema, J., Vertenstein, M., Grimmond, C.S.B., 2008. An Urban Parameterization for a Global Climate Model. Part I: Formulation and Evaluation for Two Cities. Journal of Applied Meteorology and Climatology 47, 1038–1060. https://doi.org/10.1175/2007JAMC1597.1

Oudin, L., Salavati, B., Furusho-Percot, C., Ribstein, P., Saadi, M., 2018. Hydrological impacts of urbanization at the catchment scale. Journal of Hydrology 559, 774–786. https://doi.org/10.1016/j.jhydrol.2018.02.064

Qin, Y., 2015. Urban canyon albedo and its implication on the use of reflective cool pavements. Energy and Buildings 96, 86–94. https://doi.org/10.1016/j.enbuild.2015.03.005

https://doi.org/10.5194/egusphere-2026-551
Preprint. Discussion started: 20 March 2026

Redon, E., Lemonsu, A., Masson, V., 2020. An urban trees parameterization for modeling microclimatic variables and thermal comfort conditions at street level with the Town Energy Balance model (TEB-SURFEX v8.0). Geosci. Model Dev. 13, 385–399. https://doi.org/10.5194/gmd-13-385-2020

Rigo, G., Parlow, E., 2007. Modelling the ground heat flux of an urban area using remote sensing data. Theor. Appl. Climatol. 90, 185–199.

Schär, C., Fuhrer, O., Arteaga, A., Ban, N., Charpilloz, C., Girolamo, S.D., Hentgen, L., Hoefler, T., Lapillonne, X., Leutwyler, D., Osterried, K., Panosetti, D., Rüdisühli, S., Schlemmer, L., Schulthess, T.C., Sprenger, M., Ubbiali, S., Wernli, H., 2020. Kilometer-Scale Climate Models: Prospects and Challenges. Bulletin of the American Meteorological Society 101, E567–E587. https://doi.org/10.1175/BAMS-D-18-0167.1

Segura, H., Pedruzo-Bagazgoitia, X., Weiss, P., Müller, S.K., Rackow, T., Lee, J., Dolores-Tesillos, E., Benedict, I., Aengenheyster, M., Aguridan, R., Arduini, G., Baker, A.J., Bao, J., Bastin, S., Baulenas, E., Becker, T., Beyer, S., Bockelmann, H., Brüggemann, N., Brunner, L., Cheedela, S.K., Das, S., Denissen, J., Dragaud, I., Dziekan, P., Ekblom, M., Engels, J.F., Esch, M., Forbes, R., Frauen, C., Freischem, L., García-Maroto, D., Geier, P., Gierz, P., González-Cervera, Á., Grayson, K., Griffith, M., Gutjahr, O., Haak, H., Hadade, I., Haslehner, K., ul Hasson, S., Hegewald, J., Kluft, L., Koldunov, A., Koldunov, N., Kölling, T., Koseki, S., Kosukhin, S., Kousal, J., Kuma, P., Kumar, A.U., Li, R., Maury, N., Meindl, M., Milinski, S., Mogensen, K., Niraula, B., Nowak, J., Praturi, D.S., Proske, U., Putrasahan, D., Redler, R., Santuy, D., Sármány, D., Schnur, R., Scholz, P., Sidorenko, D., Spät, D., Sützl, B., Takasuka, D., Tompkins, A., Uribe, A., Valentini, M., Veerman, M., Voigt, A., Warnau, S., Wachsmann, F., Wacławczyk, M., Wedi, N., Wieners, K.-H., Wille, J., Winkler, M., Wu, Y., Ziemen, F., Zimmermann, J., Bender, F.A.-M., Bojovic, D., Bony, S., Bordoni, S., Brehmer, P., Dengler, M., Dutra, E., Faye, S., Fischer, E., van Heerwaarden, C., Hohenegger, C., Järvinen, H., Jochum, M., Jung, T., Jungclaus, J.H., Keenlyside, N.S., Klocke, D., Konow, H., Klose, M., Malinowski, S., Martius, O., Mauritsen, T., Mellado, J.P., Mieslinger, T., Mohino, E., Pawłowska, H., Peters-von Gehlen, K., Sarré, A., Sobhani, P., Stier, P., Tuppi, L., Vidale, P.L., Sandu, I., Stevens, B., 2025. nextGEMS: entering the era of kilometer-scale Earth system modeling. Geoscientific Model Development 18, 7735–7761. https://doi.org/10.5194/gmd-18-7735-2025

Seto, K.C., Güneralp, B., Hutyra, L.R., 2012. Global forecasts of urban expansion to 2030 and direct impacts on biodiversity and carbon pools. Proceedings of the National Academy of Sciences 109, 16083–16088. https://doi.org/10.1073/pnas.1211658109

Shahi, N.K., Polcher, J., Bastin, S., Pennel, R., Fita, L., 2022. Assessment of the spatio-temporal variability of the added value on precipitation of convection-permitting simulation over the Iberian Peninsula using the RegIPSL regional earth system model. Climate Dynamics 59, 471. https://doi.org/10.1007/s00382-022-06138-y

Stevens, B., Satoh, M., Auger, L., Biercamp, J., Bretherton, C.S., Chen, X., Düben, P., Judt, F., Khairoutdinov, M., Klocke, D., Kodama, C., Kornblueh, L., Lin, S.-J., Neumann, P., Putman, W.M., Röber, N., Shibuya, R., Vanniere, B., Vidale, P.L., Wedi, N., Zhou, L., 2019. DYAMOND: the DYnamics of the Atmospheric general circulation Modeled On Non-hydrostatic Domains. Prog Earth Planet Sci 6, 61. https://doi.org/10.1186/s40645-019-0304-z

Sun, Y., Zhang, N., Ao, X., Gao, Y., 2024. Numerical Studies on the Influence of Building Morphology on Urban Canopy Wind Speed. Journal of Advances in Modeling Earth Systems 16, e2023MS003881. https://doi.org/10.1029/2023MS003881

Tafasca, S., Ducharne, A., Valentin, C., 2020. Weak sensitivity of the terrestrial water budget to global soil texture maps in the ORCHIDEE land surface model. Hydrol. Earth Syst. Sci. 24, 3753–3774. https://doi.org/10.5194/hess-24-3753-2020

Van Genuchten, M.Th., 1980. A Closed-form Equation for Predicting the Hydraulic Conductivity of Unsaturated Soils. Soil Science Soc of Amer J 44, 892–898. https://doi.org/10.2136/sssaj1980.03615995004400050002x

Wonorahardjo, S., Sutjahja, I.M., Mardiyati, Y., Andoni, H., Thomas, D., Achsani, R.A., Steven, S., 2020. Characterising thermal behaviour of buildings and its effect on urban heat island in tropical areas. Int J Energy Environ Eng 11, 129–142. https://doi.org/10.1007/s40095-019-00317-0

Wouters, H., Demuzere, M., Blahak, U., Fortuniak, K., Maiheu, B., Camps, J., Tielemans, D., Van Lipzig, N.P.M., 2016. The efficient urban canopy dependency parametrization (SURY) v1.0 foratmospheric modelling: description and application with the COSMO-CLM modelfor a Belgian summer. Geosci. Model Dev. 9, 3027–3054. https://doi.org/10.5194/gmd-9-3027-2016

https://doi.org/10.5194/egusphere-2026-551
Preprint. Discussion started: 20 March 2026

Wouters, H., Demuzere, M., Ridder, K.D., Van Lipzig, N.P.M., 2015. The impact of impervious water-storage parametrization on urban climate modelling. Urban Climate 11, 24–50. https://doi.org/10.1016/j.uclim.2014.11.005

Zhao, L., Oleson, K., Bou-Zeid, E., Krayenhoff, E.S., Bray, A., Zhu, Q., Zheng, Z., Chen, C., Oppenheimer, M., 2021. Global multi-model projections of local urban climates. Nat. Clim. Chang. 11, 152–157. https://doi.org/10.1038/s41558-020-00958-8